In order to establish the generality of the concepts described in this paper, the oxidation of a cadmium amalgam in benzene containing 0.2 M $[NHx_4][ClO_4]$ or 0.2 M $[NHx_4][PF_6]$ was examined. Benzene has a lower dielectric constant than CH_2Cl_2 and is a nonpolar molecule. Thus, it would be expected to be even more weakly coordinating than CH_2Cl_2. With $[NHx_4][ClO_4]$ as the electrolyte, an $E_{1/2}$ value of 0.77 V was obtained versus $[CoCp_2]/[CoCp_2]^+$. This can be compared with a value of 1.45 V obtained in $[NHx_4][PF_6]$. Even in the presence of electrolyte, the benzene solution is of very high resistance, and all $E_{1/2}$ values are affected by ohmic *iR* drop. This factor precludes quantitative calculations of solution equilibria as was possible in CH_2Cl_2. However, the relative value of $E_{1/2}$ in $[ClO_4]^-$-containing electrolyte being 600–700 mV more negative than that in $[PF_6]^-$-containing electrolyte confirms that perchlorate is a much better ligand than hexafluorophosphate and that the combination of a poorly coordinating solvent, benzene, and a weak ligand $[PF_6]^-$ leads to an extremely positive $E_{1/2}$ value for the $Cd^{2+}/Cd(Hg)$ redox couple.

The above data imply that in CH_2Cl_2 and benzene a highly activated metal ion is produced. This hypothesis is further supported by experiments in which dimethyl sulfoxide (0.1 M) was added to CH_2Cl_2 containing $[NBu_4][PF_6]$ (0.2 M). Negative shifts in $E_{1/2}$ of 480, 440, and 160 mV were observed for data obtained at Cd, Pb, and Tl amalgam electrodes, respectively, versus the data obtained in CH_2Cl_2 containing $[NBu_4][PF_6]$ only (Table I). The shifts are attributable to the strong complexation of dimethyl sulfoxide relative to dichloromethane.

Summary

The electrochemical oxidation of Cd, Pb, and Tl mercury amalgam electrodes in noncoordinating media such as chlorinated or aromatic hydrocarbon solvents generates a highly activated form of the metal ion, which is strongly complexed by both $[ClO_4]^-$ and $[BF_4]^-$, anions that are normally regarded as noncoordinating ligands. Thus, if ligands can react at the electrode surface faster than the kinetics of precipitation, then a pathway to previously unknown complexes is available. The identification of soluble $[Cd(ClO_4)_4]^{2-}$, $[Cd(BF_4)_3]^-$, $[Pb(ClO_4)_3]^-$, $Pb(BF_4)_2$, $Tl(ClO_4)$, and $Tl(BF_4)$ complexes in dichloromethane is an example of new complexes as is the facile electrochemical synthesis of nonsolvated $Cd(BF_4)_2$.

Acknowledgment. We thank the Australian Research Grants Scheme for financial support (A.M.B.), Deakin University Research Committee for the provision of a postdoctoral research fellowship (S.R.E.), and the Commonwealth Education Department for a postgraduate scholarship (A.F.H.).

Registry No. Cd, 7440-43-9; Pb, 7439-92-1; Tl, 7440-28-0; PF_6^-, 16919-18-9; BF_4^-, 14874-70-5; ClO_4^-, 14797-73-0; Hg, 7439-97-6; CH_2Cl_2, 75-09-2; $(CH_3)_2SO$, 67-68-5; $[Cd(ClO_4)_4]^{2-}$, 104494-05-5; $[Cd(BF_4)_3]^-$, 114446-59-2; $[Pb(ClO_4)_3]^-$, 114446-60-5; $Pb(BF_4)_2$, 13814-96-5; $Tl(ClO_4)$, 13453-40-2; $Tl(BF_4)$, 28625-02-7; benzene, 71-43-2.

Simulation of Free Energy Relationships and Dynamics of S_N2 Reactions in Aqueous Solution

J.-K. Hwang, G. King, S. Creighton, and A. Warshel*

Contribution from the Department of Chemistry, University of Southern California, Los Angeles, California 90089-0482. *Received August 14, 1987*

Abstract: The energetics and dynamics of the S_N2 class of reactions in aqueous solution are studied by a combination of the empirical valence-bond (EVB) method and a free energy perturbation technique. The solvent is represented by the surface-constrained all-atom solvent (SCAAS) model, and many-body interactions are taken into account with a solvent parameter set that includes atomic polarizabilities. The EVB representation of the reaction conveniently incorporates the effect of the solvent reaction field on the polarization of the solute. The calculations evaluate the activation free energies for the $X^- + CH_3Y \rightarrow XCH_3 + Y^-$ reactions and explore the general relationship between the reaction free energies (ΔG_0) and the solvent contribution to the activation free energies (Δg^*). The simulated free energy relationship is similar to Marcus' macroscopic formula, provided that the relevant reorganization energy is estimated from the microscopic simulation. The dynamical aspects of the S_N2 charge-transfer reaction are examined by propagating trajectories downhill from the transition state and by using the linear response theory. It is found that the rather complicated solute–solvent coupling must be included in a consistent way in order to explore the nature of the reactive trajectories. The simulations indicate that the solvent fluctuations play a major role in driving the system toward the transition state and that the relaxation time for the reactive fluctuations is determined by both the polarization time of the solute dipole moment and the dielectric relaxation time of the solvent. The characteristics of the free energy fuctionals (which are the bases for phenomenological analytical models of charge-transfer reactions) are discussed, and the suitability of studying these functionals with the EVB formulation is demonstrated.

I. Introduction

The study of chemical reactions in solution has attracted significant theoretical interest in recent years (ref 1–26 provide a partial list of works and emphasize studies of charge-transfer reactions). This interest reflects in part the realization that many

(1) Warshel, A.; Russell, S. T. *Q. Rev. Biophys.* **1984**, *17*, 283.
(2) (a) Scrocco, E.; Tomasi, J. *Top. Current Chem.* **1973**, *42*, 95. (b) Tapia, O.; Poulain, E.; Sussman, F. *Chem. Phys. Lett.* **1975**, *33*, 65. (c) Rinaldi, D.; Rivail, J.-L. *Theor. Chim. Acta* **1973**, *32*, 57.
(3) (a) Warshel, A. *Chem. Phys. Lett.* **1978**, *55*, 454. (b) Warshel, A. *J. Phys. Chem.* **1979**, *30*, 285.
(4) Warshel, A.; Weiss, R. M. *J. Am. Chem. Soc.* **1980**, *102*, 6218.
(5) Pross, A.; Shaik, S. S. *Acc. Chem. Res.* **1983**, *16*, 363.
(6) (a) Shaik, S. S. *Can. J. Chem.* **1986**, *64*, 96. (b) Shaik, S. S. *J. Am. Chem. Soc.* **1987**, *106*, 1227. (c) Shaik, S. S.; Hiberty, P. C.; Lefour, J.; Ohabessian, G. *J. Am. Chem. Soc.* **1987**, *109*, 363. (d) Shaik, S. S.; Pross, A. J. *J. Am. Chem. Soc.* **1982**, *104*, 2708. (e) Shaik, S. S. *Prog. Phys. Org. Chem.* **1985**, *15*, 197.
(7) Chandrasekhar, J.; Smith, S. F.; Jorgensen, W. L. *J. Am. Chem. Soc.* **1985**, *107*, 155.
(8) Tapia, O.; Lluch, J. M. *J. Chem. Phys.* **1985**, *83*, 3971.
(9) Weiner, S.; Singh, U. C.; Kollman, P. *J. Am. Chem. Soc.* **1985**, *107*, 2219.

0002-7863/88/1510-5297$01.50/0

chemical and most biological reactions occur in the condensed phase and that gas-phase calculations cannot be expected to reliably describe condensed-phase chemistry. Although great insight into the nature of solvent effects has been provided by early macroscopic approaches (see for example ref 20 and 23–25), it seems now that obtaining reliable quantitative results requires the use of theoretical models formulated at a detailed, microscopic level. This is particularly needed in studies of charge-transfer reactions, in which the energetics and the dynamics are determined by the strong interactions between the solute and the solvent.

Despite the crucial role of the solvent in charge-transfer reactions, it is not obvious how to include the solvent in microscopic quantum mechanical calculations of such reactions. Early attempts[2,60] to represent the solvent by a macroscopic cavity could not be used for quantitative study, since the solvation energy depends in a very strong way ($1/a^3$) on the unknown cavity radius. Quantum mechanical calculations on supermolecules[12] (i.e., solute plus a limited number of solvent molecules) could not include a sufficient number of solute molecules and could not thoroughly sample the many-dimensional solvent space. The first attempt to obtain a quantitative approximation for quantum chemical calculations of charge-transfer reactions in solution involved calculations of the disassociation of a water molecule in aqueous solution.[3,4] This calculation introduced the effect of the solvent in the diagonal matrix elements of the SCF-MO Hamiltonian (MINDO-2 in this specific case) of the solute. The solvent was represented by the surface-constrained soft-sphere dipole (SCSSD) model. Later studies involved replacement of the SCF-MO method by the more reliable empirical valence-bond (EVB) method, which was implemented in both SCSSD calculations[4] and in an all-atom water model.[16a] These calculations included studies of proton transfer and general-acid catalysis reactions in aqueous solution. Similar approaches have been implemented in calculations on enzymatic reactions.[1,18,19]

Subsequent studies[7] have introduced ab initio solute potential surfaces which interact, through the calculated gas-phase charge distribution, with an all-atom water model. This approach was applied to studies of S_N2 reactions in aqueous solution. Other works based on ab initio solute surfaces and empirical solvent potential functions have emerged recently,[8-11] indicating that the field is entering a stage of rapid progress.

In view of the great interest in this exciting field and the emergence of several alternative approaches, we find it both useful and instructive to apply the EVB method to the S_N2 class of reactions. This class has become a popular test case for theoretical simulation of charge-transfer reactions in solution. This may reflect the fact that the S_N2 reactions are among the simplest charge-transfer processes, since the changes in solvation energy

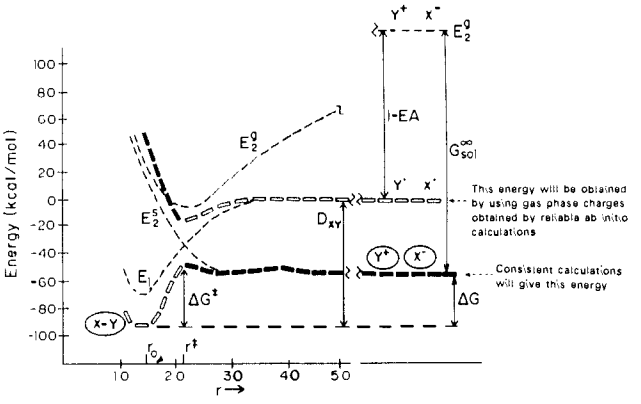

Figure 1. Demonstration of the major problems associated with using the gas-phase charge distribution. This figure considers the heterolytic cleavage of the X–Y bond in solution. This bond can be described by a mixture of a covalent state (Y–X) and an ionic state (Y^+X^-), with energies E_1 and E_2, respectively. These energies are indicated here with superscripts g and s for the gas phase and solution cases, respectively. The ground state obtained by mixing E_1^g and E_2^g becomes a pure covalent state ($Y^\cdot X^\cdot$) when the bond is broken in the gas phase. Using the gas phase charge distribution in the calculations will give zero solvation energy and an energy D_{XY} (typically 90 kcal/mol) for the bond-breaking reaction in solution (since the wave function of the bond is almost fully covalent at all points along r, the solvent does not see any dipole and will not solvate the system). On the other hand, if the solvent effect is included in the solvent Hamiltonian, one obtains a solvated ground state (Y^+X^-) for the broken bond in solution (since the solvent electrostatic stabilization lowers the energy of the ionic state and allows more ionic character in the wave function in the later half of the bond-breaking reaction). The corresponding error is around 60 kcal/mol in the case described here.

(and, thus, solvent effects) are much smaller than they are for other charge-transfer reactions (such as proton-transfer reactions). It also appears (see below) that because of its symmetric gas-phase charge distribution, the S_N2 reaction can be explored without a consistent incorporation of the solvent in the solute Hamiltonian (thus presenting a rather nonunique test case) (see below). Nevertheless, considering the fact that the S_N2 is by now a more familiar test case than the more complicated class of proton-transfer reactions,[4,16] it is useful to demonstrate the applicability of our approach to modeling this system.

The present work will explore the potential of the EVB method in studying both the energetics and dynamics of reactions in solution. In exploring the energetics of the S_N2-type reactions, we will address the general concept of linear free energy relationships. This concept is one of the cornerstones of physical organic chemistry, dating back to the Brönsted relationship[21] and to the more quantitative (yet macroscopic) formulations of Marcus[23] and Hush[24] (for reviews see ref 25 and 6). Microscopic studies of such relationships are still in their infancy. In fact, only a very limited number of microscopic studies[18] have attempted to explore this problem. The present method appears to provide a natural way to simulate free energy relationships.[18] In particular, the use of valence-bond structures (see also ref 5) allows one to evaluate from first principles the free energy functionals used in Marcus' and related theories and to examine their validity. The S_N2 systems offer a very extensive base of experimental information[25] that can be used as a consistency constraint on the simulations.

The combination of free energy calculations and quantum chemical treatments[7,16,18] is a subject of significant interest. Our approach to this problem involves a rather elaborate treatment that combines the EVB method and a free energy perturbation method. This approach might appear to some readers as an unnecessary complication considering the more recent and seemingly simpler approaches (e.g., ref 7) that used gas-phase ab initio calculations to evaluate the solute charge distribution and then calculated the solvation free energy of the frozen solute charges in the given solvent. To realize the reason for our strategy and for many of the arguments made in this paper, it is instructive

(10) Chiles, R. A.; Rossky, P. J. *J. Am. Chem. Soc.* **1985**, *106*, 6867.
(11) Kong, Y. S.; Jhon, M. S. *Theor. Chim. Acta* **1986**, *70*, 123.
(12) Creshmaschi, P.; Gamba, A.; Simonetta, M. *J. Chem. Soc. Perkin Trans. 2* **1977**, 162.
(13) (a) Adelman, S. A. *Adv. Chem. Phys.* **1983**, *53*, 61. (b) Tully, J. C. *J. Chem. Phys.* **1980**, *73*, 1975.
(14) van der Zwan, G.; Hynes, J. T. *J. Phys. Chem.* **1985**, *89*, 4181.
(15) Calef, D. F.; Wolynes, P. G. *J. Phys. Chem.* **1983**, *87*, 3400.
(16) (a) Warshel, A. *J. Phys. Chem.* **1982**, *86*, 2218. (b) Warshel, A.; Hwang, J.-K. *J. Chem. Phys.* **1986**, *89*, 4938. (c) Hwang, J.-K.; Warshel, A. *J. Am. Chem. Soc.* **1987**, *109*, 715.
(17) Lee, J.; Robinson, G. W. *J. Am. Chem. Soc.* **1985**, *107*, 6153.
(18) (a) Warshel, A. *Proc. Natl. Acad. Sci. U.S.A.* **1984**, *81*, 444. (b) Warshel, A. *Pontif. Acad. Sci. Script. Var.* **1984**, *55*, 59. (c) Warshel, A.; Russell, S. T.; Sussman, F. *Isr. J. Chem.* **1987**, *27*, 217.
(19) (a) Warshel, A.; Russell, S. T. *J. Am. Chem. Soc.* **1986**, *108*, 6595. (b) Warshel, A. *Biochemistry* **1981**, *20*, 3167. (c) Warshel, A.; Sussman, F. *Proc. Natl. Acad. Sci. U.S.A.* **1986**, *83*, 3806.
(20) Moore, J. W.; Pearson, R. G. *Kinetics and Mechanism*; Wiley: New York, 1981.
(21) Brönsted, J. N.; Pederson, K. *Z. Phys. Chem.* **1924**, *108*, 185.
(22) Hammond, G. S. *J. Am. Chem. Soc.* **1955**, *77*, 334.
(23) (a) Marcus, R. A. *J. Phys. Chem.* **1968**, *72*, 891. (b) Marcus, R. A. *Annu. Rev. Phys. Chem.* **1964**, *15*, 155.
(24) Hush, N. S. *J. Chem. Phys.* **1958**, *28*, 296.
(25) Albery, J. W.; Kreevoy, M. M. *Adv. Phys. Org. Chem.* **1978**, *16*, 87.
(26) Kurz, J. L.; Kurz, L. C. *Isr. J. Chem.* **1985**, *26*, 339.

to consider the heterolytic bond cleavage described in Figure 1 (see also ref 4). The figure demonstrates why a completely rigorous gas-phase calculation will produce a charge distribution that will lead to a very large error in calculating the dissociation energy in solutions. This crucial point, which is not so obvious in cases of S_N2 reactions, emphasizes the need for a consistent coupling between the solvent charge distribution and the solute polarization.

The coupling between the solvent charge distribution and the solute charge distribution determines the energetics of the charge-transfer reactions and thus strongly influences the dynamics of these reactions.[16a] Understanding the actual nature of this coupling could be crucial in determining the dynamics of a given reaction and the corresponding reaction pathway.[26] Although very significant progress has been made in experimental studies of charge-transfer reactions,[27-31] it is difficult to "invert" the experimental information in a unique way to obtain the corresponding microscopic parameters. Here again it seems essential to augment the experimental information and the available phenomenological models through microscopic simulations of these systems.

Attempts to simulate the actual microscopic dynamics of charge-transfer reactions in polar solvents were confined until recently to EVB studies of proton-transfer and electron-transfer reactions[16] and to chemical reactions in proteins.[18] The EVB method appears to provide an effective way for studying the coupling between the solute and solvent coordinates. This coupling is entirely different for diabatic and adiabatic processes. Approaches that explicitly include the interacting electronic states provide a convenient way of exploring the two limiting cases. The simpler diabatic limit, in which the mixing between the relevant charge-transfer states is small, was explored by a semiclassical trajectory approach.[16a,b] The adiabatic limit, however, requires more extensive studies, since in this case a simple separation of the solute and solvent fluctuations cannot be assumed. Simulating S_N2 reactions might provide a powerful theoretical benchmark for various analytical models.

Section II of this paper describes our theoretical formulation, outlining the convenient analytical potential surfaces and their implementation in free energy calculations and in dynamical simulations. This part also examines some formal aspects of the relationship between the reaction rate constants and the fluctuations of the solvent. Section III presents the results of our simulations, emphasizing both the examination of linear free energy relationships and the dynamical response of the solvent to the dipole moment of the solute. Our main conclusions are discussed in section IV.

II. Methods

(a) Analytical Potential Surfaces for the Solute–Solvent Systems. This section will describe the EVB procedure for the specific case of an S_N2 reaction (eq 1).

$$X^- + CH_3Y \rightarrow XCH_3 + Y^- \qquad (1)$$

In this system there are three atomic orbitals that are the most important in determining the potential energy surface for the reaction. These are the atomic p_z orbitals centered on the X, Y, and C atoms (see Figure 2a). For the sake of simplicity in this paper we make a number of assumptions regarding the quantum mechanics of the S_N2 reaction: (1) We assume that the three orbitals in Figure 2a are the dominant orbitals. Treating them separately from the rest of the orbitals in the system does not change the reaction potential energy surface in any major way. (2) It is assumed that the hybridization of the three oritals does not change over the course of the reaction and specifically that the $2p_z$ orbital on the central carbon atom does not mix with the 2s orbital. (This is of course not a very good assumption but any errors can be absorbed into the empirical matrix elements described later.) (3) We neglect

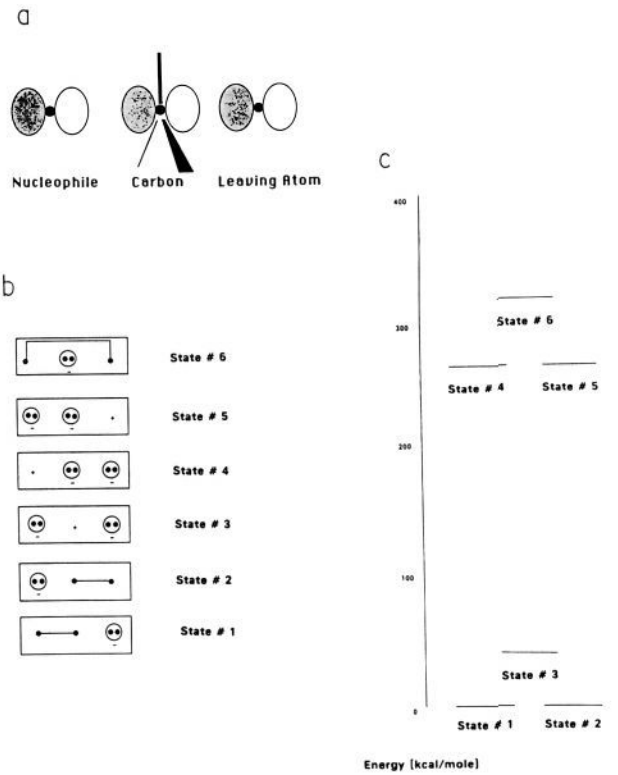

Figure 2. (a) Three active p_z orbitals that are used in the quantum treatment of the S_N2 reaction. (b) Valence-bond diagrams for the six possible valence-bond states for four electrons in three active orbitals. (c) Relative approximate energy levels of the valence-bond states in the gas phase with the three quantum atoms in a geometry where the X–C and C–Y distances are 2.0 Å and the X–Y distance is 4.0 Å. See Table I for the estimation of these energies.

quantum interaction between the three "active" atomic orbitals and the other orbitals in the system (e.g., C–H bonds and the lone-pair orbitals on the X and Y atoms). (4) The contribution to the reaction potential energy surface of the remaining orbitals is evaluated by a classical force field method (i.e., using harmonic bond and angle terms to attempt to mimic the actual quantum mechanical potential energy terms).

We could use an SCF-MO formalism to determine the energy of the system as a function of the coordinates of the X, Y, and C atoms over the course of the substitution reaction. However, there are bonds broken in the reaction, and it is well-known that the SCF-MO methods fail when treating bond-breaking processes.[58] Thus, we must use a formalism that will effectively treat bond breaking. Any method allowing for more than one Slater determinant (configuration) in the wave function will work. Some possible choices are the CI, MCSCF, and VB methods, with all of these approaches being exactly equivalent in the limit of a complete basis set of configurations. (Our system has 4 electrons in three orbitals so the complete basis set will have six Slater determinants; see Figure 2b.) We prefer to use the VB method since the form of the wave function of each of the configurations has direct chemical meaning. This allows one to safely neglect some of the configurations to a first approximation, when inspection of the bonding diagram (Figure 2b) indicates that these configurations have high energy. Another advantage of the VB method is that the distribution of charge in each configuration is obvious (i.e., the atomic orbitals have either 0, 1, or 2 electrons with no fractional occupancy). This feature allows the electrostatic coupling between the classical solvent and the VB configurations to be treated easily.

For this paper we will use only the three configurations corresponding to the states

$$\phi_1 = X{:}^- C{-}Y \qquad \phi_2 = X{-}C\ Y{:}^- \qquad \phi_3 = X{:}^-\ C^+\ Y{:}^- \qquad (2)$$

These three states have the lowest energy of the six possible states of the 4-electron three-orbital system. The other three states have very high energy: The two states $X{:}^-C{:}^-Y^+$ and $X^+C{:}^-Y{:}^-$ have an unfavorable juxtaposition of negative charges as well as a positive charge on a halogen atom; the other state $X^{\bullet}C{:}^-Y^{\bullet}$ has an almost completely broken bond as well as a carbanion (see Table I and Figure 2c). In a fuller treatment of the reaction we would need to use these resonance structures to recover all of the correlation energy, but for the approximate empirical treatment

(27) Kosower, E. M.; Huppert, D. *Annu. Rev. Phys. Chem.* **1986**, *37*, 127.
(28) Werst, D. W.; Londo, W. F.; Smith, J. L.; Barbara, P. F. *Chem. Phys. Lett.* **1985**, *118*, 367.
(29) McGuire, M.; Mclendon, G. *J. Phys. Chem.* **1986**, *90*, 2549.
(30) Hicks, J.; Vandersall, M.; Barbarogic, Z.; Eisenthal, K. B. *Chem. Phys. Lett.* **1985**, *116*, 18.
(31) Kenny-Wallace, G. A.; Quitevis, E. L.; Templeton, G. *Rev. Chem. Intermed.* **1985**, *6*, 197.

Table I. "Back of the Envelope" Estimation of the Energies of the Valence-Bond States (kcal/mol)

Data Used in Calculating the Energies of the States[a]

parameter	value	abbrev
average halogen atom		
ionization potential	250	IP_X
electron affinity	70	EA_X
methyl group		
ionization potential	230	IP_{CH_3}
electron affinity	$\simeq 0$[b]	EA_{CH_3}
carbon–halogen covalent bond[c]	60	$D_{C\text{-}X}$
4.0-Å halogen–halogen bond[d]	0	$D_{X\text{-}X}$
+−− charge distribution energy[e]	−60	$V_{QQ}(+--)$
−+− charge distribution energy[e]	−180	$V_{QQ}(-+-)$

Approximate Valence-Bond State Energies[f]

$E(1)$ = reference state energy = 0
$E(2)$ = reference state energy = 0
$E(3) = V_{QQ}(-+-) + IP_{CH_3} - EA_X + D_{C\text{-}X} = +40$
$E(4) = V_{QQ}(+--) + IP_X - EA_{CH_3} + D_{C\text{-}X} = +250$
$E(5) = V_{QQ}(+--) + IP_X - EA_{CH_3} + D_{C\text{-}X} = +250$
$E(6) = IP_X - EA_{CH_3} + D_{C\text{-}X} - D_{X\text{-}X} = +310$

[a] See ref 64 for typical numbers. [b] Reference 65. [c] Rough estimate of the energy of an average C–X bond at 2.0 Å (see ref 64). [d] The bond is assumed to be almost completely broken. [e] Coulomb energy of the given charge distribution at the transition-state geometry. [f] Neglecting induced dipole and delocalization effects. The numbers are only a rough guideline and are not meant to be taken too seriously.

we plan to use, these structures should have negligible effect due to their very high energy.

The VB wave functions corresponding to active electrons in these states are given in (3), where the vertical bars denote Slater determinants and the notation Y_α indicates the orbital on the atom Y has an electron with α spin. The N's denote normalization constants.

$$\phi_1 = N_1\{|Y_\alpha C_\beta X_\alpha X_\beta| - |Y_\beta C_\alpha X_\alpha X_\beta|\}$$
$$\phi_2 = N_3\{|Y_\alpha Y_\beta C_\alpha X_\beta| - |Y_\alpha Y_\beta C_\beta X_\alpha|\}$$
$$\phi_3 = N_2|Y_\alpha Y_\beta X_\alpha X_\beta| \quad (3)$$

Since this is an approximate treatment of the S_N2 reaction, we will limit ourselves to these three low-energy states and define our basis for the electronic wavefunction as (4).

$$\Phi_1 = \phi_1\chi_1 \qquad \Phi_2 = \phi_2\chi_2 \qquad \Phi_3 = \phi_3\chi_3 \quad (4)$$

The basis wave functions given above are product functions of the valence-bond wavefunctions given earlier and the functions χ_i, which are the wave functions for the other inactive electrons in the problem moving in the field defined by the active electrons. We have thus partitioned the molecular electronic space into active and inactive parts, and we assume no interaction between these parts. This requires that the Hamiltonian be of the form $H = H_{act} + H_{inact}$. The matrix elements between the basis wave functions are as in (5). The active electron matrix elements given

$$H_{ii} = \langle\Phi_i|H|\Phi_i\rangle = \langle\phi_i|H_{act}|\phi_i\rangle + \langle\chi_i|H_{inact}|\chi_i\rangle$$
$$H_{ij} = \langle\Phi_i|H|\Phi_j\rangle = \langle\phi_i|H_{act}|\phi_j\rangle + \langle\chi_i|H_{inact}|\chi_j\rangle \quad (5)$$

in ref 59 are as in (6)

$$\langle\phi_1|H_{act}|\phi_1\rangle = (1 + S_1^2 - S_2^2)^{-1}(\langle\mathbf{1}|H_{act}|\mathbf{1}\rangle + \langle\mathbf{1}|H_{act}|\mathbf{2}\rangle - \langle\mathbf{1}|H_{act}|\mathbf{3}\rangle)$$
$$\langle\phi_2|H_{act}|\phi_2\rangle = (1 - S_1^2 + S_2^2)^{-1}(\langle\mathbf{5}|H_{act}|\mathbf{5}\rangle - \langle\mathbf{5}|H_{act}|\mathbf{6}\rangle + \langle\mathbf{5}|H_{act}|\mathbf{7}\rangle)$$
$$\langle\phi_3|H_{act}|\phi_3\rangle = \langle\mathbf{4}|H_{act}|\mathbf{4}\rangle$$
$$\langle\phi_1|H_{act}|\phi_3\rangle = (2/(1 + S_1^2 - S_2^2))^{1/2}\langle\mathbf{1}|H_{act}|\mathbf{4}\rangle$$
$$\langle\phi_3|H_{act}|\phi_2\rangle = (2/(1 - S_1^2 + S_2^2))^{1/2}\langle\mathbf{4}|H_{act}|\mathbf{7}\rangle$$
$$\langle\phi_1|H_{act}|\phi_2\rangle = (2/(1 - (S_1^2 - S_2^2)^2))^{1/2}\langle\mathbf{1}|H_{act}|\mathbf{5}\rangle \quad (6)$$

where $\mathbf{1} \equiv Y(1)C(2)X(3)X(4)$, $\mathbf{2} \equiv C(1)Y(2)X(3)X(4)$, $\mathbf{3} \equiv Y(1)X(2)X(3)C(4)$, $\mathbf{4} \equiv Y(1)Y(2)X(3)X(4)$, $\mathbf{5} \equiv Y(1)Y(2)C(3)X(4)$, $\mathbf{6} \equiv Y(1)C(2)Y(3)X(4)$, $\mathbf{7} \equiv Y(1)Y(2)X(3)C(4)$, $S_1 \equiv \langle Y|C\rangle$, and $S_2 \equiv \langle X|C\rangle$.

X, Y, and C are the wave functions of the atomic p_z orbitals on the X, Y, and C atoms, respectively. This formulation assumes that the overlap integral and exchange integral between the p_z orbitals on the atoms X and Y are negligable. See ref 59 for evaluation of these matrix elements.

The matrix elements of the inactive electrons are evaluated by a classical force field and are given in (7). The meanings of these terms will be discussed below.

$$\langle\chi_i|H_{inact}|\chi_i\rangle = \tfrac{1}{2}\sum_{angles} K_\theta^{(i)}(\theta - \theta_0^{(i)})^2 + \tfrac{1}{2}\sum_{bonds} K_b^{(i)}(b - b_0^{(i)})^2 + V_{nonbonded}^{(i)} \quad (7)$$
$$\langle\chi_i|H_{inact}|\chi_j\rangle = 0$$

Our task at this stage is to obtain analytical expressions for the matrix elements of the Hamiltonian and then to evaluate the ground-state potential surface, E_g, through the relationship (eq 8), where S is the overlap matrix ($S_{ij} = \langle\psi_i|\psi_j\rangle$).

$$\mathbf{C}_g^\dagger(\mathbf{S}^{-1/2}\mathbf{H}\mathbf{S}^{1/2})\mathbf{C}_g = \mathbf{C}_g^\dagger\mathbf{H}\mathbf{C}_g = E_g \quad (8)$$

The usual EVB procedure involves diagonalizing this 3 × 3 Hamiltonian. However, here we use a very simple model for the S_N2 reaction and will represent the potential surface and wave function of our reacting system using only two electronic states. Using a two-state system will preserve most of the important features of the potential energy surface while at the same time providing a simple model of the S_N2 reaction that will be more amenable to discussion than the three-state system. For our two-state system we define the states in (9) as our reactant and product wave functions. For this paper the vector R can be assumed to be ($R_{X\text{-}C}$, $R_{C\text{-}Y}$).

$$\psi_1 = \alpha_1(\mathbf{R})\Phi_1 + \beta_1(\mathbf{R})\Phi_3 \qquad \psi_2 = \alpha_2(\mathbf{R})\Phi_2 + \beta_2(\mathbf{R})\Phi_3 \quad (9)$$

The mixing of state 3 into states 1 and 2 can be visualized as the polarization of the covalent bond in each structure as the nucleophile brought up to the carbon. In the product and reactant states with the nucleophile at infinite separation from the carbon center (i.e., $R_{prod,max} = (1.5, \infty)$ or $R_{reac,max} = (\infty, 1.5)$), there will be a net polarization of the covalent bond due to the difference in the electronegativity of the two atoms. In the gas phase, as the nucleophile approaches the carbon its negative charge increases the bond polarity since the electronegativity of the carbon is reduced by the presence of a nearby negative charge. However, in solution phase the energies of states 1 and 2 are lowered with respect to the energy of state 3 even more than they are in the gas phase, and this polarization term is expected to have smaller dependence on the nuclear coordinates than in the gas phase. In a first approximation we can assume that the α's and β's do not depend on R and that they are equal to the coefficients of the ionic and covalent terms in the valence-bond wave function of the C–X and C–Y bonds.

The matrix elements of our 2 × 2 active Hamiltonian are then given as (10).

$$H_{11}^0 = \langle\psi_1|H|\psi_1\rangle = \alpha_1^2\langle\Phi_1|H|\Phi_1\rangle + \beta_1^2\langle\Phi_2|H|\Phi_2\rangle + 2\alpha_1\beta_1\langle\Phi_1|H|\Phi_2\rangle \quad (10)$$
$$H_{22}^0 = \langle\psi_2|H|\psi_2\rangle = \alpha_2^2\langle\Phi_3|H|\Phi_3\rangle + \beta_2^2\langle\Phi_2|H|\Phi_2\rangle + 2\alpha_2\beta_2\langle\Phi_3|H|\Phi_2\rangle$$
$$H_{12}^0 = \langle\psi_1|H|\psi_2\rangle = \alpha_1\alpha_2\langle\Phi_1|H|\Phi_3\rangle + \alpha_1\beta_2\langle\Phi_1|H|\Phi_2\rangle + \alpha_2\beta_1\langle\Phi_2|H|\Phi_3\rangle + \beta_1\beta_2\langle\Phi_2|H|\Phi_2\rangle$$

These matrix elements are in a form that can be evaluated by standard quantum chemical methods. This evaluation is tedious, and the earlier assumpitons that we made will lead to errors in the matrix elements. On the other hand, we can use experimental information to approximate the diagonal matrix elements. That is, the rather complicated function H_{11} will be given, at the range where $R_{X\text{-}C}$ is large compared to the C–Y bond length, by a Morse potential function that depends on the distance $R_{C\text{-}Y}$. When X^- approaches C, we have a repulsive van der Waals interaction and an attractive charge-induced dipole interaction between these atoms. We can describe both of these forces using analytical potential energy terms (see below). The same argument applies to H_{22}. As far as H_{12} is concerned, we can approximate it by an exponential term and fit the parameters in this term to the experimental information on the gas-phase potential energy surface of the reaction or, if needed, to accurate gas-phase calculations (e.g., ab initio CI,[63] MCSCF,[62] or VB[32-34]). Note that this approach compensates for our approximate formal treatment as, for

(32) Goddard, W. A., III; Dunning, T. H., Jr.; Hunt, W. J.; Hay, P. J. *Acc. Chem. Res.* **1973**, *6*, 368.
(33) Cooper, D. L.; Gerratt, J.; Raimondi, M. *Nature (London)* **1986**, *323*, 699.
(34) Epiotis, N. D. *Theory of Organic Reaction*; Springer-Verlag: Berlin, 1978.
(35) Warshel, A.; King, G. *Chem. Phys. Lett.* **1985**, *121*, 124.

Table II. Parameters for the Potential Functions[a,e] Parameters of Solute–Solute Interactions

Bonded Function Parameters[b]

atoms	D	$^1/_2K_b$	b_0	a
C–Cl	60.0		1.8	2.0
C–H		310.6	1.102	

Nonbonded Function Parameters[c]

atoms	ϵ^*	r^*	A^c	B^c	μ
C, Cl^-	0.1459	3.1500			
Cl, Cl^-	0.1366	5.5866			
H, Cl^-			11297.2	120.45	3.6

Bending Potential Function Parameters[d]

atoms	$^1/_2K_\theta$	θ_0
H–C–H	36.0	109.5
H–C–Cl	30.0	109.5

EVB Matrix[e]

	A	μ	r_0
H_{12}	22.0	1.0	5.0

Parameters of Water–Water and Water–Solute Interaction

atom	q	A_i[f]	B_i[f]	γ[g]
H	0.328	6.14	1.650	0.1
O	−0.656	648.5	23.17	1.23
H[h]	0.410	5.0	2.000	
O[h]	−0.820	793.3	25.02	
F^-	−1.000	11000.0	2.501	
Cl^-[h]	−1.000	2000.0	2.501	
Cl^-	−1.000	15000.0	2.501	
I^-	−1.000	16000.0	2.501	

[a] Energies in kilocalories/mole; distances in angstroms. [b] The bonded energy is given either by Morse potential. $D\exp[-2a(b-b_0)] - 2\exp[-a(b-b_0)]$ or by harmonic potential $^1/_2K_b(b-b_0)^2$. [c] The nonbonded interaction is given either by $\epsilon^*[(r^*/r)^{12} - 2(r^*/r)^6]$ or by $A\exp(-\mu r) - B/r^6$. [d] The bending function is given by $^1/_2K_\theta(\theta-\theta_0)^2$. [e] The EVB off-diagonal element H_{12} is given by $A\exp(-\mu(r-r_0))$. [f] The solute–water van der Waals interaction is given by $A_iA_j/r^{12} - B_iB_j/r^6$. [g] γ is the atomic polarizability. [h] Parameters used for calculations without including induced dipole.

example, the Morse potential is the *exact* form of H_{22} at $R_{prod,max}$. Other semiempirical SCF methods attempt to fit only *atomic* terms (e.g., resonance and repulsion integrals) to experiments, while our method fits the matrix elements of well-defined *states* to direct experimental information about the potential energy surface (fitting the diagonal matrix elements to the known bond length, bond energies, nonbonded interactions, and electrostatic energies). Thus, we feel that this method is inherently more reliable than other semiempirical quantum mechanical methods.

The method described above is intended to show the motivation for an *approximate* two-state description of the S_N2 reaction. It is not intended to be a rigorous derivation of the two-state model. The model used is the simplest possible one that includes most of what we feel is the major physics behind solute polarization in solution. We refer the readers to ref 62 and references therein for a deeper discussion of the quantum chemical significance of adopting a two-state model for chemical reactions. Moreover, our treatment is *not at all restricted to a two-state model*. The same EVB treatment has been used before for three or more states.[19a] We feel that the two-state model is the simplest and most efficient way to present our approach.

In view of the above arguments, we concentrate on fitting the gas-phase information to the two-state model in (11) in which the gas-phase

$$\epsilon_1^0 = H_{11}^0 = M(b_1) + V_{nb}^{(1)} + V_{ind}^{(1)} + \tfrac{1}{2}\sum_m K_b^{(1)}(b_m^{(1)} - b_0)^2 + \tfrac{1}{2}\sum_m K_\theta^{(1)}(\theta_m^{(1)} - \theta_0)^2 \quad (11)$$

$$\epsilon_2^0 = H_{22}^0 = M(b_2) + V_{nb}^{(2)} + V_{ind}^{(2)} + \alpha^{(2)} + \tfrac{1}{2}\sum_m K_b^{(2)}(b_m^{(2)} - b_0)^2 + \tfrac{1}{2}\sum_m K_\theta^{(2)}(\theta_\theta^{(2)} - \theta_0)^2$$

$$H_{12} = A\exp[-\mu(r_3 - r_3^0)]$$

energies ϵ_i^0 are represented by a rather standard force field (of the type discussed in ref 53), where b_1, b_2, and r_3 are the X–C, C–Y, and X–Y distances, $M(b_j)$ is the Morse potential for the jth bond, b_m are the C–H bond lengths, and θ_m are the X–C–H, H–C–H, and H–C–Y angles defined by the covalent bonding arrangement for a given resonance structure. For example, in ψ_1 the θ_m are defined by the H–C–Y and H–C–H angles, and the K_θ for the X–C–H angles are set to zero. The $V_{nb}^{(i)}$ are the nonbonded interactions between the nonbonded atoms in the ith resonance structure. For ψ_1 this includes the $X^-\cdots C$ repulsion, the $X^-\cdots H$ repulsion, and the $X^-\cdots Y$ interaction. The nonbonded interactions are described by either $Ae^{-\mu r}$ or 6–12 van der Waals potential functions (see Table II). The induced dipole terms describe the attraction between the charges of the system (Q) and its induced dipoles. This is evaluated (kcal/mol) by

$$V_{ind}^{(i)} = -166\sum_m \gamma_m|\xi_m^{(i)}|^2 \quad (12)$$

where $\xi_m^{(i)}$ is the vacuum field on the mth atom from the charges ($\xi_m^{(i)} = \Sigma_j Q_j^{(i)} r_{mj}/r_{mj}^3$) with the system in state ψ_i, and γ_m is the atomic polarizability of the mth atom. The induced dipole–induced dipole interactions are neglected in the solute potential. Finally, the $\alpha^{(2)}$ parameter is the energy difference between ψ_2 and ψ_1 with the fragments at infinite separation (this is simply the difference in heat of formation of $X^- + CH_3Y$ and $Y^- + CH_3X$). The parameters used are given in Table II.

The key point about the functional form of ϵ_1 and ϵ_2 is that the experimental properties of the reactants and products at infinite separation are reproduced exactly. The behavior at the transition-state region can then be obtained by adjusting H_{12} to fit calculations and/or experiments. The gas-phase potential surface used in this paper for the Cl^- CH_3Cl system is shown in Figure 3. This surface presents the best fit obtained with the two-state model to the ab initio calculations[7] of the barrier and to an experimental estimate of the ion–dipole complexation energy. Our barrier is 3.6 kcal/mol as compared to the ab initio result of 3.6 kcal/mol and −5 kcal/mol for the complexation energy as compared to the −8.6 kcal/mol observed complexation energy and to ab initio calculations[7] ranging between −14.9 and −10.3 kcal/mol. A better fit could be obtained by the three-state model (eq 2), but such a treatment would complicate our discussion with little additional benefit.

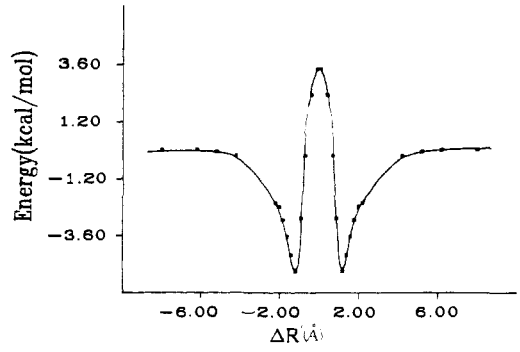

Figure 3. Gas-phase EVB potential surface for the Cl^- + $CH_3Cl \rightarrow ClCH_3 + Cl^-$ reaction. The reaction coordinate $\Delta R'$, which is determined by minimum energy reaction pathway, is given by $\Delta R' = b_2 - b_1$, where b_2 is the distance between C and leaving Cl and b_1 is the distance between C and nucleophile Cl. See the text for a discussion of the relation between this surface and the available experimental and theoretical information.

The main point in the EVB method is not in its gas-phase surface but in its treatment of the solvent. The formal treatment of the solute–solvent system can be done by writing the wave function of the system as a product of the solute and solvent wave functions as in (13), where ϕ are

$$\Phi_{i,m}^0 = \psi_i\phi_1^0\phi_2^0\cdots\phi_m^j\cdots\phi_n^0 \quad (13)$$

the wave functions of the solvent molecules and ϕ_m^j designates that the mth solvent molecule is in its jth excited state. Neglecting charge-transfer interaction between the solvent and solute, we can treat the solvent molecules classically (as was done for the inactive electrons of the solute). Such treatment takes into account the effect of the excited solvent molecules by a perturbation treatment and results in a classical interaction between the solute charges and the solvent-induced dipoles (see Appendix 4 of ref 1). Thus, we can write the diagonal matrix elements of the solute–solvent system as the sum of the gas-phase matrix element for the solute and a term that represents the classical interaction between the solute and the solvent. The off-diagonal term should be influenced by the solvent also; in particular, it includes the coupling of states ψ_1 and ψ_2 with ψ_3, and the energy difference between these states depends on the solvent configuration at any given moment of time. However, since the energy gaps between states 1–3 and 2–3 are large, we will neglect the effect of the solvent on the matrix element H_{12} to a

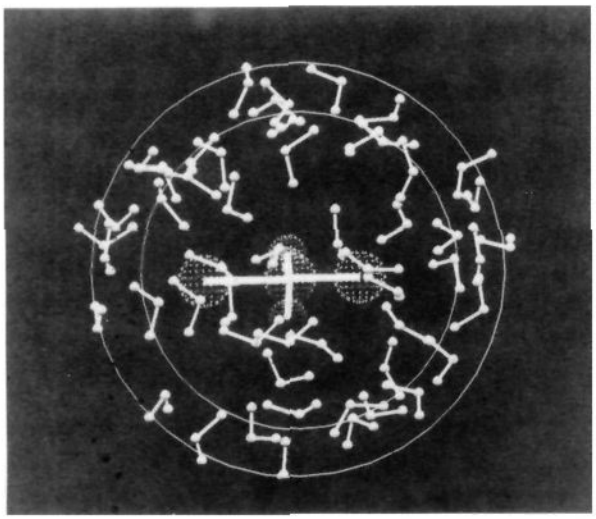

Figure 4. "Snapshot" of one of the many configurations generated by molecular dynamics simulation of an SCAAS + EVB model of the Cl^- + $CH_3Cl \rightarrow ClCH_3 + Cl^-$ S_N2 reaction. This configuration is generated on the potential $\epsilon_m = (\epsilon_1 + \epsilon_2)/2$, which constrains the system to be at the transition-state region.

first approximation and set it equal to its gas-phase value.[56] That is, we use (14), where S and s designate solute and solvent, respectively. V_{Qq}

$$\epsilon_1 = H_{11} = H_{11}^0 + V_{Qq,Ss}^{(1)} + V_{nb,Ss}^{(1)} + V_{ind,Ss}^{(1)} + V_s \quad (14)$$

$$\epsilon_2 = H_{22} = H_{22}^0 + V_{Qq,Ss}^{(2)} + V_{nb,Ss}^{(2)} + V_{ind,Ss}^{(2)} + V_s$$

$$H_{12} = H_{12}^0$$

is the electrostatic interaction between the solute charges (Q) in the given resonance structure and the solvent residual charges (q), V_{nb} is the nonbond interaction between solute and solvent atoms, and V_{ind} is the interaction of the solvent induced dipoles with the solute charges (eq 15).

$$V_{Qq} = 332 \sum_{i(S)j(s)} Q_i q_j / r_{ij} \quad (15)$$

$$V_{nb} = \tfrac{1}{2}\sum_{i \neq j} (A_i A_j / r_{ij}^{12} - B_i B_j / r_{ij}^{6})$$

$$V_{ind} = -166 \sum_{j(s)} (\gamma_j / d)|\xi_j|^2 =$$

$$-166 \sum_{j(s)} (\gamma_j / d)\left|\sum_{k(s)} q_k r_{jk} / r_{jk}^3 + \sum_{i(S)} Q_i r_{ji} / r_{ji}^3\right|^2$$

Here the field ξ on each solvent atom includes the effect of both the solute and the solvent charges. The screening constant d accounts for the attenuation of the field due to induced dipole–induced dipole interactions. The replacement of the self-consistent treatment of the interaction between induced dipoles by the use of the screening constant is examined elsewhere (e.g., ref 1). The solvent–solvent interaction is modeled by charge–charge and 6–12 potentials and induced-dipole terms (which are included in V_{ind}). The inclusion of the solvent-induced dipoles allows us to use the gas-phase charge distribution in assigning the residual charges for the solvent atoms. However, for the purpose of comparison with other treatments, we will also consider a parameter set without induced dipoles. All the solvent parameters are listed in Table II.

In treating the solvent molecules, we introduce spherical boundary conditions using the surface-constrained all-atom solvent (SCAAS) model, which is described in detail elsewhere[35] and outlined in Figure 4. This model surrounds the reactive region with a sphere of solvent molecules. The surface of this solvent sphere is constrained by additional forces that simulate the effect of the missing bulk solvent.

With analytical functions for ϵ_1, ϵ_2, and H_{12} we can now obtain an analytical surface for the solute–solvent system by diagonalizing **H**. This gives (16). The nature of this analytical surface can best be understood

$$E_g = \tfrac{1}{2}[(\epsilon_1 + \epsilon_2) - [(\epsilon_1 - \epsilon_2)^2 + 4H_{12}^2]^{1/2}] \quad (16)$$

from Figure 5. As seen from the figure, the reactant state is favored when the solvent molecules are polarized toward X and the product state is favored when the solvent is polarized toward Y. The solvent will act to push down the energy of either state by dipole–charge interactions, thus adding a new coordinate to the potential energy surface of the reacting molecule, the solvent coordinate. This coordinate can be conveniently represented as the difference of the interaction energy of state 1 and state 2 with the solvent. In the gas phase, this coordinate always has a value of 0 and the potential energy surface of the system depends only on the nuclear coordinates of the solute. The multidimensional nuclear and electronic solvent coordinate can be projected onto this one-dimensional energy gap, which represents the extent to which the solvent is polarized toward one solute charge distribution or the other. It is instructive to note that this solvent polarization strongly influences the solute charge distribution at any given solute nuclear geometry. This is because the solvent will shift the energies of the two electronic states relative to their gas-phase values, and this causes the mixture of states 1 and 2 in the actual electronic wave function to deviate from the gas-phase mixture. Thus, at any given solute geometry, the ground state in Figure 5a has more negative charge on X and that in Figure 5b has more negative charge on Y. This polarization effect has an important but not dominant role in the S_N2 reaction, but for charge separation reactions (e.g., proton transfer in solution) it will be a dominant factor since it allows the solute to respond to the solvent polarization by changing its polarization, thus influencing the solvent motion. This is also the main reason that gas-phase potential energy could lead to inconsistent results in solution—they have no information about the effect of the solvent fields on the solute charge distribution.

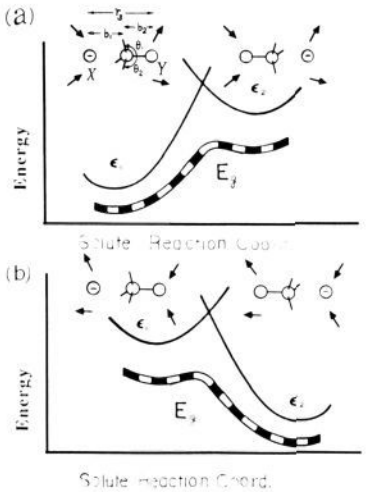

Figure 5. Relationship between the polarization of the solvent dipoles and the energetics of the diabatic states (ϵ_i) and adiabatic ground state (E_g) for the S_N2 reaction $X^- + CH_3Y \rightarrow XCH_3 + Y^-$. When the solvent dipoles are polarized toward X (upper figure), the reactant state, ψ_1, is stabilized. When the solvent dipoles point toward Y (lower figure), the product state, ψ_2, is stabilized. For any given solute geometry the ground state in the upper figure has more negative charge on X than in the ground state of the lower figure.

(b) Evaluating Activation Free Energies. Once the analytical potential surface is constructed, it is possible to evaluate the reaction rate by running molecular dynamics trajectories and finding the number of times the system reaches its transition state. This, however, would require an extremely long simulation time except for systems with low activation barriers. Fortunately, one can express the relevant rate constant[36,37] by (17), where $\beta = (k_B T)^{-1}$ and k_B is the Boltzmann constant. k_{TST} is the

$$k = F k_{TST} = F(k_B T/h) \exp[-\Delta g^{\ddagger}\beta] \quad (17)$$

rate constant given by the standard transition-state theory[36] and F is the transmission factor that contains all the true dynamical information (see next section). The factor $\exp[-\Delta g^{\ddagger}\beta]$ expresses the probability that the system will be in the transition-state region $\Delta X^{\ddagger}$ relative to the probability of being in an equal increment of the reaction coordinate at the reactant state. The problem is to evaluate the activation free energy, $\Delta g^{\ddagger}$, for the quantum mechanical ground-state surface E_g. An effective method that allows one to tackle this problem is provided by a combination of the EVB method and a free energy perturbation technique. The details of this method are given elsewhere.[18b,c] Here, we will outline the main points and a recent modification that improves the rate of convergence.

Our task is to find the probability that the system will be at the yet to be defined transition state. This requires an effective way of forcing the system to spend a significant amount of time in selected regions of

(36) Glasstone, S.; Laidler, K. J.; Erving, H. *The Theory of Rate Processes*; McGraw-Hill: New York, 1941.
(37) Anderson, J. B. *J. Chem. Phys.* **1973**, *58*, 4684.

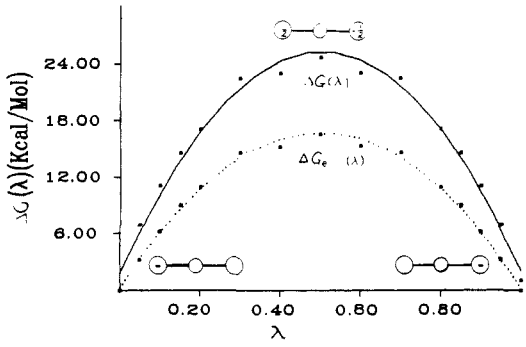

Figure 6. Parametric dependence of the mapping free energy on the parameter λ. The figure shows both the total free energy $\Delta G(\lambda)$ (solid line) and the electrostatic contribution $\Delta G_{el}(\lambda)$ (dotted line). The figure demonstrates that the largest contribution to $\Delta G(\lambda)$ is due to electrostatic interactions.

configuration space. The EVB method provides a very convenient mapping potential for doing this, and the free energy perturbation method tells us how to evaluate the free energy change associated with the mapping process (see below). Unfortunately, none of our mapping potentials coincide with the actual ground-state potential. Thus, we take a two-step strategy starting with a convenient mapping procedure and then using the relevant raw data to construct the ground-state free energy surface.

We start by performing a series of simulations using a potential of the form (18) and changing the vector $\lambda^m = (\lambda_1^m, \lambda_2^m)$ in a systematic way from (1, 0) to (0, 1) in n small increments, where the index m is changed from 0 to $n-1$. In this way we can drive the system from the reactant

$$\epsilon_m = \lambda_1^m\epsilon_1 + \lambda_2^m\epsilon_2 - 2(\lambda_1^m\lambda_2^m)^{1/2}|H_{12}| \qquad \lambda_1^m + \lambda_2^m = 1 \qquad (18)$$

state through the transition state and into the product state. Note that ϵ_1 has a minimum at the reactant geometry and ϵ_2 has a minimum at the product geometry so that as we change m, we force the system to move from the reactant state to the product state. Specifically, the solvent is forced to adjust its polarization to the changing charge distribution of the solute, and we will be able to see how much free energy the solvent needs to adjust to the solute configuration by using the free energy perturbation formalism described below.

The H_{12} term, which was not used in our previous studies, minimizes the difference between the mapping potential and the actual ground-state potential. That is, the convergence of the calculated ground-state free energy depends (see below) on a correction term involving the difference between E_g and ϵ_m. Thus, we use an ϵ_m that is as close as possible to E_g. Unfortunately, the ground-state potential is given by the complicated function (eq 8 and 19), where the C_g's are implicit functions of the H_{ij}'s.

$$E_g = \mathbf{C}_g\mathbf{H}\mathbf{C}_g = \sum_{ij} C_{gi}C_{gj}H_{ij} \qquad (19)$$

As the simulation proceeds, the eigenvector $\mathbf{C}_g$ fluctuates in an unpredictable way, making it hard to use it for generating a mapping potential. However, replacing $\mathbf{C}_g$ by a constant vector $\mathbf{C}_m$, with $C_{mi} = (\lambda_i^m)^{1/2}$, produces (with $\lambda_1 = \lambda_2 = 0.5$) a potential ϵ_m that approaches E_g at the transition-state region, where $C_{g1} \simeq C_{g2} = 1/(2^{1/2})$. This guarantees stable results at the transition-state region.

The free energy associated with changing ϵ_1 to ϵ_2 may be obtained with the relationship[38,39] (20), where $\langle\ \rangle_m$ indicates an average of the quantity within the brackets calculated on potential surface ϵ_m, and the free energy

$$\delta G(\lambda_m \rightarrow \lambda_{m'}) = -(1/\beta)\ \ln\ [\langle\exp(-(\epsilon_{m'} - \epsilon_m))\beta\rangle_m] \qquad (20)$$

$$\Delta G(\lambda_n) = \Delta G(\lambda_0 \rightarrow \lambda_n) = \sum_{m=0}^{n-1} \delta G(\lambda_m \rightarrow \lambda_{m+1})$$

functional $\Delta G(\lambda)$ reflects both the electrostatic solvation effects associated with the changes of the solute charges as well as the intramolecular effects associated with changing ϵ_1 to ϵ_2. Figure 6 demonstrates the dependence of $\Delta G(\lambda)$ on λ for an exchange reaction where X = Y. The figure gives both the total $\Delta G(\lambda)$ and its electrostatic components.

Obtaining $\Delta G(\lambda)$ with the perturbation procedure using the mapping potentials ϵ_m is not sufficient for evaluating the activation free energy, Δg^*, which reflects the probability of being at the transition state on the actual ground-state potential surface. The quantity $\Delta G(\lambda)$ is basically used to find the free energy associated with changing ϵ_1 to the potential ϵ_m^* that forces the system to spend the longest time near the actual transition state. However, one still needs to find the probability of reaching the transition state for trajectories that move on E_g. The corresponding formulation (which is described in detail elsewhere[16c,18c]) defines the reaction coordinate X^n in terms of the energy gap $\epsilon_2 - \epsilon_1$. This is done by dividing the configuration space of the system into subspaces, S^n, that satisfy the relationship $\Delta\epsilon(S^n) = X^n$, in which the energy differences X^n are constants and $\Delta\epsilon = \epsilon_2 - \epsilon_1$. The X^n are then used as the reaction coordinate, giving

$$\exp[-\Delta g(X^n)\beta] = \exp[-\Delta G(\lambda_m)\beta]\langle\exp[-(E_g(X^n) - \epsilon_m(X^n))\beta]\rangle \qquad (21)$$

This expression relates the probability of finding the system at X^n on the ground state E_g in terms of the probability of being on the mapping potential ϵ_m that keeps X around X^n. The evaluation of $\Delta g(X^n)$ for an exchange reaction is described in Figure 8. In addition to $\Delta g(X^n)$, we can obtain the probability of being at X^n on ϵ_1. This probability defines the free energy functionals, Δg_i ($\Delta g_i(X^n) = \int\exp[-\epsilon_i(X^n)\beta]\ dS^n$), which can be obtained through the same derivation that led to eq 21, and are given by (22). The evaluation of the Δg_i functionals for an exchange reaction is demonstrated in Figure 7.

$$\exp[-\Delta g_i(X^n)\beta] = \exp[-\Delta G(\lambda_m)\beta]\langle\exp[-(\epsilon_i(X^n) - \epsilon_m(X^n))\beta]\rangle_m \qquad (22)$$

This work attempts to evaluate free energy relationships on a microscopic level (the actual calculations are described in section III). To examine simple analytical approximations for the calculated dependence of Δg^* on ΔG_0, we consider the harmonic expansion of our diabatic surface. This expansion can be obtained from the power spectra of the time-dependent $\epsilon_i(t)$ as was done in our dispersed polaron model[16a] and gives (23), where the R's and Q's are the dimensionless coordinates for

$$\epsilon_1 \simeq \sum_i(\hbar/2)\omega_r^i(r_i + \Delta_r^i/2)^2 + \sum_j(\hbar/2)\omega_q^j(q_j + \Delta_q^j/2)^2 \simeq (\hbar/2)\omega_R(R + \Delta_R/2)^2 + (\hbar/2)\omega_Q(Q + \Delta_a/2)^2 \qquad (23)$$

$$\epsilon_2 \simeq \sum_i(\hbar/2)\omega_r^i(r_i - \Delta_r^i/2) + \sum_j(\hbar/2)\omega_q^j(q_j - \Delta_q^j/2)^2 + \Delta V_0 \simeq (\hbar/2)\omega_R(R - \Delta_R/2)^2 + (\hbar/2)\omega_Q(Q - \Delta_Q/2)^2 + \Delta V_0$$

the solute and the solvent, respectively. The effective frequencies ω_Q and ω_R are evaluated by $\omega = \int_0^\infty\omega\ P(\omega)\ d\omega$ in which $P(\omega)$ is the normalized power spectrum of the corresponding contribution to $(\epsilon_2 - \epsilon_1)$. The R are related to the regular reaction coordinate $R' = (b_1 - b_2)$ by $R = R'(\omega_R\mu_R/\hbar)^{1/2}$ where μ_R is the reduced mass for the normal mode that is

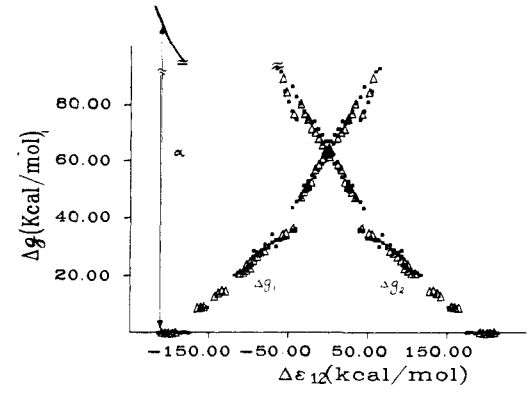

Figure 7. Free energy functionals, Δg_1 and Δg_2 (see also ref 16c), as a function of the energy gap $\Delta\epsilon$. The calculations are done with (●) and without (△) solvent-induced dipoles.

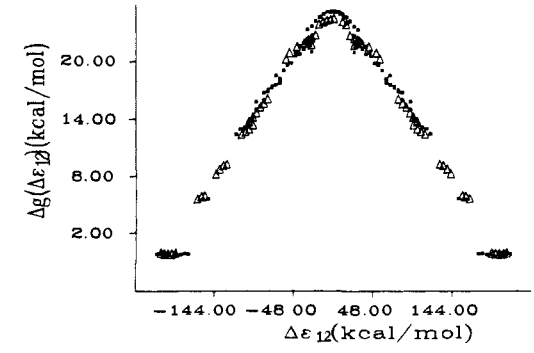

Figure 8. Actual free energy profile for the ground-state surface as a function of the energy gap $\Delta\epsilon$. The calculations are done for the $Cl^- + CH_3Cl \rightarrow ClCH_3 + Cl^-$ exchange reaction, with (●) and without (△) solvent-induced dipoles.

the compression of b_1 and the extension of b_2. The reaction coordinate Q is defined in terms of the electrostatic contribution $(\epsilon_2 - \epsilon_1)_{el}$ to $(\epsilon_2 - \epsilon_1)$. Thus, we have $Q = (2(\epsilon_2 - \epsilon_1)_{el}/\hbar\omega_Q)^{1/2}$, which is also related to the regular solvent coordinate, Q', by $Q = Q'(\omega_Q m_Q/\hbar)^{1/2}$. ΔV_0 is the difference between the minima of ϵ_2 and ϵ_1. Here we replace the contribution from each set of coordinates by one effective coordinate. The displacements Δ's are related to the so-called reorganization energy, α, given by (24).

$$\alpha = \alpha_R + \alpha_Q = \sum_i (\hbar/2)\omega_r^i(\Delta_r^i)^2 + \sum_j (\hbar/2)\omega_q^j(\Delta_q^j)^2 \simeq (\hbar/2)\omega_R\Delta_R^2 + (\hbar/2)\omega_Q\Delta_Q^2 \quad (24)$$

In the harmonic case we can evaluate the activation potential from eq 16 and 23, obtaining (25), where the first terms represents the difference between the value of ϵ_1 at the transition state and the minimum of ϵ_1 at

$$\Delta V^\ddagger \simeq (\Delta V_0 - \alpha)^2/4\alpha - H_{12}(X_0)^2/\alpha - H_{12}(X^\ddagger) \qquad |\alpha| > |\Delta V_0| \quad (25)$$

X_0 (this term is simply obtained by finding the intersection of the two diabatic parabolas). The second term is the difference between the minima of ϵ_1 and E_g, and the last term is the difference between the values of ϵ_1 and E_g at the transition state. The validity of eq 25 for anharmonic systems and its more physical form, where the ϵ_i is replaced by the corresponding Δg_i, are discussed in section III.

(c) Studying Dyamical Effects. A consistent description of the dynamics of charge-transfer reactions in polar solvents is far from being a simple task. Major problems are associated with the dependence of the solvation energy on the solute reaction coordinate, as well as the necessity to describe the reaction in terms of several electronic surfaces. The simplest case appears to be associated with electron-transfer reactions, in which H_{12} is small. In such a case one can consider the dynamics on a single diabatic surface (e.g., ϵ_1) and evaluate the surface-crossing probability at the transition-state region, where $\Delta\epsilon$ approaches zero. This gives the rate constant in terms of the probability of reaching the transition state and a Landau–Zener-type transmission factor.[16b] Dynamical effects can be conveniently extracted (using a cumulant expansion) from the autocorrelation function of the energy gap $\Delta\epsilon(t)$. Here, however, the situation is far more complicated; H_{12} is large, and one must run trajectories on the adiabatic potential surface where the solute dipole moment varies along the reaction coordinate. In such cases one has to consider the mutual solute–solvent polarization, and the corresponding formal treatments are inherently complicated (see Appendices A and B). One can still use numerical approaches, provided the potential surface is given by an analytical expression. Such an analytical expression is provided by the EVB ground-state energy (eq 16), which captures the key electrostatic coupling between the solvent and the solute.

To explore dynamical effects, one would like to evaluate the transmission factor F of eq 17 as a function of the solvent dielectric relaxation time. Numerical simulation of F can be obtained conveniently by propagating trajectories first on $\epsilon_{m^\ddagger}$ and then switching the potential surface to E_g and continuing the trajectories. Monitoring the downhill trajectories whose initial momentum at $X^\ddagger$ points from the reactant state to the product state gives one a direct estimate of F, by the fraction of these trajectories that arrive in the product state.[37] The transmission factor can also be evaluated in terms of the reactive flux autocorrelation function.[54,55,61]

The overall dynamics may also be studied by a less explicit treatment, considering the projection of the actual many-dimensional dynamics on a space of lower dimensionality. In particular, it is instructive to consider the dynamics in two dimensions in terms of one effective solute coordinate (R) and one effective solvent coordinate (Q). Such effective coordinates are conveniently defined by the R and Q of eq 23 in terms of the corresponding solvent and solute contributions to $\epsilon_2 - \epsilon_1$. An equivalent and more familiar definition of the solvent coordinate can be obtained in terms of the macroscopic reaction field (ξ_R) at the solute cavity, i.e., taking Q to be proportional to ξ_R we obtain (26), where $(\epsilon_2 - \epsilon_1)_{el}$ is the electrostatic contribution to $(\epsilon_2 - \epsilon_1)$, μ_1 and μ_2 are the dipole moments of the solute for the corresponding diabatic states, and $Q = \xi_\parallel/C$ (where $\xi_\parallel$ is the projection of ξ on $(\mu_1 - \mu_2)$.

$$(\epsilon_2 - \epsilon_1)_{el} = (\mu_1 - \mu_2)\xi_R = CQ(\mu_1 - \mu_2) \quad (26)$$

Once the coordinates are selected, we need a convenient description of the corresponding effective potential. As stated above one can describe the diabatic surfaces ϵ_1 and ϵ_2 in terms of shifted harmonic potentials (eq 23). Our problem, however, is to describe the *actual* ground-state adiabatic potential in terms of Q and R. Fortunately, the dependence of E_g on the solvent coordinate can be written in the simple way without eq 16. This can be done by considering the solvent interaction with the adiabatic ground-state dipole moment of the solute (eq 27), where the ground-state

$$E_g(Q) = V(Q) \simeq (\hbar/2)\omega_Q Q^2 - \mu\xi_R = (\hbar/2)\omega_Q Q^2 - CQ\mu \quad (27)$$

$$\mu = \mu_1 + (\mu_{max}/2)(1 - \cos 2\theta) \quad (28)$$

adiabatic dipole moment, μ, is given by[40] eq 28 and where $\cot 2\theta = (\epsilon_2 - \epsilon_1)/2H_{12}$ and $\mu_{max} = (\mu_2 - \mu_1)$. The parameter C can be related to the solvent reorganization energy α_Q by eq 29, where we assume that $|H_{12}/\alpha| \ll 1$ so that μ is given by μ_1 and μ_2 at $-\Delta_Q/2$ and $\Delta_Q/2$, respectively (the

$$\alpha_Q = V_Q(Q = \Delta_Q/2) - V_Q(Q = -\Delta_Q/2) = \mu_2 C(\Delta_Q/2) - \mu_1 C(-\Delta_Q/2) = -C(\Delta_Q/2)\mu_{max} \quad (29)$$

same result can be obtained by comparing eq 26 and 23 and the relationship $\alpha_Q = (\hbar/2)\omega_Q\Delta_Q^2$). Thus, we obtain eq 30.

$$V(Q) = (\hbar/2)\omega_Q Q^2 - (2\alpha_Q/\Delta_Q)(\mu/\mu_{max})Q \quad (30)$$

With the potential of eq 30 one can write the equation of motion for the solvent coordinate as[41] (31), where $A'(t)$ is a random force and m_Q

$$m_Q\ddot{Q}' = -\int_0^t m_Q\gamma_Q(t-\tau)\,\dot{Q}'(\tau)\,d\tau - \partial V/\partial Q' + A'(t) \quad (31)$$

is defined in Appendix A. Approximating γ_Q by a δ function ($\gamma = \gamma_Q \delta(t)$) and using the dimensionless coordinate, $Q = (m_Q\omega_Q/\hbar)^{1/2}Q'$, eq 31 can be written as (32), where $A(t) = (\omega_Q/\hbar m_Q)^{1/2} A'(t)$. We can use

$$\ddot{Q} = -\gamma_Q\dot{Q} - \omega_Q^2 Q - (\omega_Q/\hbar)(2\alpha_Q/\Delta_Q)[(\partial\mu/\partial Q)Q + \mu]/\mu_{max} + A(t) \quad (32)$$

the properties of the Brownian harmonic oscillator (Appendix A) to relate γ_Q to the autocorrelation function (acf) of $Q(t)$, while $A(t)$ can be related to γ_a by the fluctuation dissipation theorem.

Similarly, we can write the approximate equation of motion of R as (33).

$$\ddot{R} = -\gamma_R\dot{R} - (\omega_R/\hbar)\partial E_g/\partial R + A_R(t) \quad (33)$$

The coupled equations (32 and 33) can be expressed in terms of the equivalent Smoluchowski equation and solved under simplified conditions (Appendix A). It is also interesting to attempt to solve these equations numerically by Langevin dynamics. Here, however, we prefer to explore the nature of reactive trajectories in (Q, R) space using linear response theory. The rationale is based on the following intuitive argument. The rate constant can be written as[66,67] (34a), where $H(\dot{X})$ is 1 and 0 for

$$k = \langle \dot{X}H(\dot{X})\xi\rangle^\ddagger \exp[-g(X^\ddagger)\beta]/\int \exp[-g(X)\beta]\,dX = (\langle\dot{X}_+\rangle^\ddagger/\Delta X^\ddagger)\int_{X^\ddagger-\Delta X^\ddagger}^{X^\ddagger} \exp[-g(X)\beta]\,dX/\int \exp[-g(X)\beta]\,dX = (\langle\dot{X}_+\rangle/\Delta X^\ddagger)\exp[-\Delta g^\ddagger\beta] \quad (34a)$$

positive and negative $\dot{X}$, respectively, and ξ is a factor that counts each productive trajectory only once and is taken as $1/m$ for a productive trajectory that crosses the transition state m times[67] (for some different formulations see also ref 55 and 61). The notation $\langle\dot{X}_+\rangle$ designates the average of $\langle\dot{X}\,H(\dot{X})\,\xi\rangle$. The quantity $(\langle\dot{X}_+\rangle/\Delta X^\ddagger)^{-1}$ is the average time it takes for a productive trajectory to pass $\Delta X^\ddagger$, and we can write (34b).

$$k \simeq \bar{\tau}^{-1}\exp[-\Delta g^\ddagger\beta] \quad (34b)$$

The time $\bar{\tau}$ is not much different from the time it takes a downhill trajectory to move from the transition state to the product state. $\bar{\tau}$ can be determined if we know the time dependence of the average solvent coordinate for productive trajectories and use the approximate relationship (35). The time derivative of $\langle Q_+\rangle$ reflects the solvent dielectric

$$\bar{\tau}^{-1} = (\partial\langle Q(t)_+\rangle/\partial t)/\Delta Q^\ddagger \quad (35)$$

relaxation time (see below) and therefore relates the rate constant to the solvent dynamical properties. Maybe more importantly, one can use $\langle Q_+(t)\rangle$ to explore the mechanistic features of the reaction coordinate outside the transition-state region. Specifically, the relationship between $\langle Q(t)\rangle$ and $\langle R(t)\rangle$ can be used to define reactions as either "solvent driven" or "solute driven". With eq 35 in mind we can evaluate $\langle Q(t)\rangle$ by propagating many downhill trajectories or alternatively using the

(38) Zwanzig, P. W. *J. Chem. Phys.* **1954**, *22*, 1420.
(39) Valleau, J. P.; Torrie, G. M. In *Modern Theoretical Chemistry*; Berne, B., Ed.; Plenum: New York, 1972; Vol. 5, p 137.
(40) Davydov, A. S. *Quantum Mechanics*; Pergamon: Oxford, 1976.

linear response theory.[41] This can be done by noting that the driving force in the equation of motion for the solvent coordinate can be described in terms of the zeroth-order solvent Hamiltonian and a perturbation Hamiltonian H' given by (36). According to linear response theory[41] we have (37).

$$H' = (\omega_Q/\hbar)(2\alpha_Q/\mu_{max}\Delta_Q)\mu Q \simeq F_{ext}Q = A\mu Q \quad (36)$$

$$\langle Q(t)\rangle = -A\beta\int_0^t \langle\dot{Q}(0)\, Q(t')\rangle\mu(t-t')\, dt' \quad (37)$$

If the acf of $Q(t)$ can be represented by a single exponential we will have (38). Describing the time dependence of the solute dipole moment

$$\langle Q(0)\, Q(t)\rangle = B\exp[-t/\tau_Q]$$

$$-\frac{d}{dt}\langle Q(0)\, Q(t)\rangle = \langle\dot{Q}(0)\, Q(t)\rangle = (B/\tau_Q)\exp[-t/\tau_Q] \quad (38)$$

with a relaxation time τ_μ ($\mu = \mu_1(1-\exp(-t/\tau))$, we obtain the recursive approximation (39), where $(\tau^*)^{-1} = (\tau_Q^{-1} - \tau_\mu^{-1})$ and $\tau_\mu^{(n-1)}$ is the re-

$$\langle Q(t)\rangle_n = -(AB\beta\mu_1/\tau_Q)\int_0^t \exp[-(t-t')/\tau_Q](1-\exp[-t'/\tau_\mu^{(n-1)}]\, dt') = ((Q'(\infty))/\tau_Q)(\tau_Q - \tau^*\exp[-t/\tau_\mu^{(n-1)}] - (\tau_Q - \tau^*)\exp[-t/\tau_Q]) \quad (39)$$

laxation time obtained by evaluating the time-dependent solute coordination using eq 33 with the $\langle Q(t)\rangle_{n-1}$ obtained in the previous iteration of eq 39.

In the special case of $\tau_L = \tau_\mu$, eq 40 holds.

$$\langle Q(t)\rangle = ((Q(\infty))/\tau_L)(\tau_L + (t-\tau_L)\exp[-t/\tau_L]) \quad (40)$$

This interesting behavior is different from that obtained in related studies of fluorescence line shifts.[50,51] The difference reflects the fact that in realistic adiabatic systems the development of the dipole μ takes a finite time. Attempts to evaluate $\langle Q(t)\rangle$ are reported in section III.

Other options of studying dynamical effects are considered in Appendices A and B. The main point (for related studies see ref 14, 15, 16b, 47, and 48) is that the dynamical effects can be extracted from acf of the time-dependent energy gap. The solvent contribution to the acf is characterized on a macroscopic level by the longitudinal dielectric relaxation time. Our interest, however, is to explore the validity of the macroscopic estimates on a microscopic level.

III. Results and Discussion

(a) Free Energy Surfaces and Free Energy Relationships. To evaluate the free energy surface of our reaction, it is necessary to sample the configuration space of the solute–solvent system along its reaction coordinate. We performed this sampling with molecular dynamics simulations, using our molecular simulation package MOLRIS. The solute (nucleophile + a methyl halide) and a surrounding cluster of 60 water molecules constituted the system we studied. (A preliminary study using 80 water molecules yielded similar results.) The potential energy surface of the entire system was evaluated with the SCAAS model[35] for the water, and the EVB parameters of Table II for the solute. The SCAAS model applies surface-constraint forces (to maintain the correct surface polarizataion and solvent density) and Brownian forces to the solvent molecules at or near the surface, which for this work were the outermost 34 molecules. The frictional and stochastic components of the Brownian force are adjusted so as to provide a "thermostat" for the system. For the present simulations the average temperature was maintained at $\simeq$300 K. Trajectories of 4 ps were collected for each of a number of points along the solute reaction coordinate (after equlibration runs of $\simeq$6 ps) with a time step of 0.6 fs. Each 4-ps trajectory required 8 h of cpu time on a VAX 11/780. The free energy change associated with moving from state m to state m' was taken as the average of the forward and backward processes, $(\Delta G_{mm'} - \Delta G_{m'm})/2$, with $\Delta G_{mm'}$ (forward) and $\Delta G_{m'm}$ (backward) defined as in eq 20. The convergence errors of our similations were assessed by integrating the free energy change of the forward and backward processes and found to be less than 1 kcal/mol.

As a first test case we consider the $Cl^- + CH_3Cl \rightarrow ClCH_3 + Cl^-$ exchange reaction. The gas-phase potential surface, which was obtained by fitting the two-state gas-phase EVB calculations to the corresponding ab initio barrier[7] and the experimental complexation energy,[52] is given in Figure 3 (see discussion in Methods). The free energy for this reaction is solution was obtained with our mapping procedure, and the results are described in Figures 6–8. Figure 6 describes the free energy associated with changing the mapping potential ϵ_m of eq 18 from ϵ_1 to ϵ_2. The electrostatic contribution to this free energy has been calculated by retaining only the electrostatic terms of ϵ_m (the solute–solvent interaction). The resulting free energy function reflects the change in the free energy of the solute charges during the reaction and is also given in Figure 6. The increase in the electrostatic free energy for $\lambda = (1, 0) \rightarrow \lambda = (^1/_2, ^1/_2)$ is due to the spreading of the solute charge over two centers and can be estimated without any simulation by scaling the corresponding macroscopic expression. For $\lambda = (1, 0)$ we basically have the solvation free energy of an isolated Cl^- ion, which can be evaluated by "fitting" the Born equation to the observed solvation free energy of a Cl^- ion, using (41) with energy in kilocalories per mole and the effective cavity

$$\Delta G_{sol}(Cl^-) \simeq -166(Q^2/\bar{a}) = -166/\bar{a} = -70 \quad (41)$$

radius a in angstroms. Using the observed $\Delta G_{sol}(Cl^-)$ to obtain $\bar{a}$, rather than using $\bar{a}$ to obtain ΔG_{sol}, allows one to eliminate some of the arbitrary nature associated with the ill-defined cavity radius.[1]

(41) Kubo, R. *Rep. Prog. Theor. Phys.* **1966**, *29*, 255.
(42) Nee, T. W.; Zwanzig, R. *J. Chem. Phys.* **1970**, *52*, 6353.
(43) (a) Szabo, A.; Schulten, K.; Schulten, Z. *J. Chem. Phys.* **1980**, *72*, 4350. (b) Schulten, K.; Schulten, Z.; Szabo, A. *J. Chem. Phys.* **1981**, *74*, 4426.
(44) (a) The longitudinal relaxation time, $\tau_L = 0.23$ ps, of water is calculated by $\tau_L = \tau_D(2\epsilon_\infty + 1)/(2\epsilon_0 + 1)$ where $\epsilon_\infty = 78.6$ and $\epsilon_0 = 1.8$ are the low- and high-frequency dielectric constants and $\tau_D = 8$ ps is the Debye relaxation time.[44b] (b) Davies, M. In *Dielectric Properties and Molecular Behavior*; Hill, N. E., Vaughan, W. E., Price, A. H., Davies, M., Eds.; van Nostrand-Reinhold: New York, 1969.
(45) Wang, M. C.; Uhlenbeck, G. E. *Rev. Mod. Phys.* **1945**, *17*, 323.
(46) Kramers, H. A. *Physica* **1940**, *7*, 284.
(47) Ovchinnikova, M. Ya. *Sov. J. Chem. Phys.* **1986**, *4*, 1.
(48) Zusman, L. D. *Chem. Phys.* **1980**, *49*, 295.
(49) Feynman, R. P.; Hibbs, A. R. (1965) *Quantum Mechanics and Path Integrals*; McGraw-Hill: New York, 1965.
(50) Mazurenko, Y. T.; Bakshiev, N. G. *Opt. Spectrosc.* **1970**, *28*, 490.
(51) Bagchi, B.; Oxtoby, D. W.; Fleming, G. R. *Chem. Phys.* **1984**, *86*, 257.
(52) Dougherty, R. C.; Roberts, J. D. *Org. Mass Spectrom.* **1974**, *8*, 77.
(53) Warshel, A. *Modern Theoretical Chemistry*; Segal, G., Ed.; Plenum: New York, 1977; Vol. 7.
(54) Yamamoto, T. *J. Chem. Phys.* **1960**, *33*, 281.
(55) Chandler, D. *J. Chem. Phys.* **1978**, *68*, 2959.
(56) The approximation involved in keeping H_{12} in solution at its gas-phase value does neglect off-diagonal contributions of the solvent-induced dipoles (that can be evaluated by an exciton-type formalism). Similarly, we neglect in our formulations electronic overlap (and therefore charge transfer) between the solvent and solute molecules. It is also important to point out that the neglect of the solvent effect on the off-diagonal terms is common to all works using gas-phase potential surfaces. However, the VB treatment *does not neglect* the first-order effect on the solute Hamiltonian (this seems to be the dominant effect of the solvent on the solute charge distribution).
(57) Warshel, A.; Weiss, R. M. *J. Am. Chem. Soc.* **1979**, *101*, 6131.
(58) Slater, J. C. *Quantum Theory of Molecules and Solids*; McGraw-Hill: New York, 1963; Vol. 1.
(59) Coulson, C. A.; Danielsson, U. *Ark. Fys.* **1954**, *25*, 245.
(60) Salem, L. *Electrons in Chemical Reactions: First Principles*; Wiley: New York, 1982; p 228.
(61) Montgomery, J. A.; Chandler, D.; Berne, B. J. *J. Chem. Phys.* **1979**, *70*, 4056.
(62) Bernardi, F.; Robb, M. A. *J. Am. Chem. Soc.* **1984**, *106*, 54.
(63) Shaik, S. S. *J. Am. Chem. Soc.* **1981**, *103*, 3692.
(64) Huheey, J. E. *Inorganic Chemistry*, 2nd ed.; Harper & Row: New York, 1978.
(65) Benson, S., private communication.
(66) Grimmelmann, E. K.; Tully, J. C.; Helfand, E. *J. Chem. Phys.* **1981**, *74*, 5300.
(67) Bennett, C. H. In *Algorithms for Chemical Computation*; Christofferson, R. E., Ed.; American Chemical Society: Washington, DC, 1977.

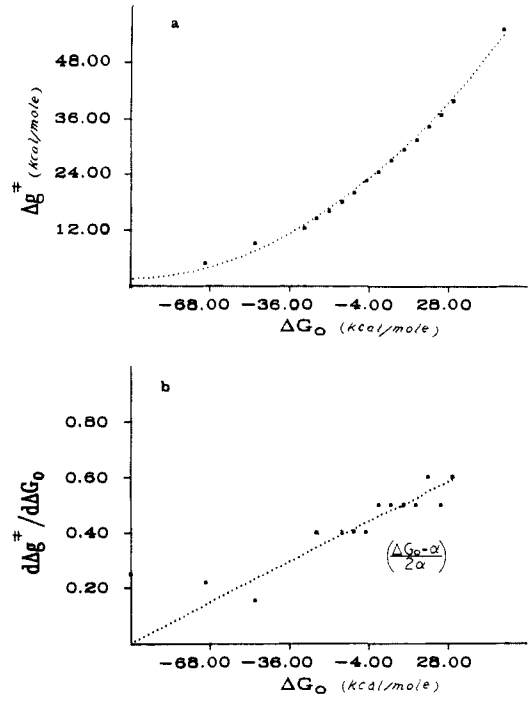

Figure 9. (a) Relationship between the activation free energy $\Delta g^{\ddagger}$ and the reaction free energy ΔG_0. (b) Dependence of the "linear" correlation coefficient $d\Delta g^{\ddagger}/d\Delta G_0$ on ΔG_0.

For $\lambda = (^1/_2, ^1/_2)$ we have charges of −0.5 on each of the Cl atoms, separated by a distance R. The corresponding energy is given by[1]

$$\Delta G_{sol}(R) + 332Q_1Q_2/R \simeq \Delta G_{sol}(R = \infty) + 332Q_1Q_2/\epsilon R \simeq \Delta G_{sol}(R = \infty) + (332/4)/80R \simeq \Delta G_{sol}(R = \infty) \quad (42)$$

$\Delta G_{sol}(R = \infty)$ can be estimated with the scaled $\bar{a}$ of eq 41 as

$$\Delta G_{sol}(R = \infty) = -166(Q_1^2 + Q_2^2)/\bar{a} = -(166/2)/(-166/\Delta G_{sol}(Cl^-)) = \Delta G_{sol}(Cl^-)/2 \quad (43)$$

This gives

$$\Delta G_{sol}(R) \simeq \Delta G_{sol}(Cl^-)/2 - 332/4R = -35 - 332/4R \quad (44)$$

with

$$\Delta G(\lambda^{\ddagger}) = \Delta G(\lambda = ^1/_2) - \Delta G(\lambda = 1) = \Delta G_{sol}(R^{\ddagger}) - \Delta G_{sol}(Cl^-) = -\Delta G_{sol}(Cl^-)/2 - 332/4R^{\ddagger} \quad (45)$$

With $R^{\ddagger} = 4.6$ Å, one obtains $\Delta G(\lambda^{\ddagger}) = -53 - (-70) = 17$ kcal/mol as compared to the value of 16.6 kcal obtained by our mapping potential. The mapping free energy $\Delta G(\lambda)$ is converted by eq 21 to the actual ground-state free energy $\Delta g(\Delta\epsilon)$, which is shown in Figure 8. The calculated activation barrier, $\Delta g^{\ddagger}$, is similar to the experimentally observed barrier ($\Delta g_{calcd}^{\ddagger} = 26.0$ kcal/mol, $\Delta g_{obsd}^{\ddagger} = 26.6$ kcal/mol). As mentioned before,[16] the difference between the barrier in solution and in the gas phase is largely due to the corresponding change in solvation free energy. Another important factor in determining the free energy surface for this reaction is the influence of the solvent polarization on the solute charge distribution. This point will be discussed below.

With a reasonable model we can explore several fundamental issues. In particular, it is interesting to examine the dependence of the activation free energy on the free energy of the reaction. The EVB method allows one to address this problem in a very convenient way. For instance, changing $\alpha^{(2)}$ in eq 11 changes in a parametric way the free energy difference, ΔG_0, between the reactant and product states. Evaluating the $\Delta g^{\ddagger}$ that corresponds to the various ΔG_0's allows one to study the underlying free energy relationship on a microscopic level.[16c,18b,c] Such a study is described in Figure 9, which presents the calculated microscopic dependence of $\Delta g^{\ddagger}$ on ΔG_0 for an hypothetical system where all the potential parameters except $\alpha^{(2)}$ are set at their values for the $Cl^- + CH_3Cl \rightarrow ClCH_3 + Cl^-$ system. This corresponds to a variation of the electronegativity of the atom while its ionic radius is kept constant. Our computer experiments provide a convenient data base for examination of various phenomenological models. In particular, it eliminates the need for finding a common denominator for experiments with different X's and Y's, as the change of ligands involves changes in many parameters (e.g. H_{12}), which makes a direct comparison to a macroscopic model far from being simple. For example, the corresponding analysis would require a careful comparison to the relevant gas-phase experiments in order to extract the solvent contribution.

As seen from the figure, the dependence of $\Delta g^{\ddagger}$ on ΔG_0 is quite monotonic and can be described as (46), where θ changes from around 1 for very endothermic reactions to 0.5 for $\Delta G_0 \simeq 0$ and

$$\Delta\Delta g^{\ddagger} = \theta\Delta\Delta G_0 \quad (46)$$

then to 0 for very exothermic reactions. The change of θ from around 1 for the case of a productlike transition state to around 0 for reactantlike transition state has been predicted by many phenomenological approaches.[21-25] However, the main point in our approach is not in finding the universal θ, but examining its microscopic nature.

A formal starting point can be provided by eq 25. Obviously this equation is useful for estimating $\Delta g^{\ddagger}$ only if the system is nearly harmonic and if $\Delta g^{\ddagger}$ is close to $\Delta V^{\ddagger}$. In this respect, it is important to mention that our Δg_1 and Δg_2 surfaces are *not* equal to ϵ_1 and ϵ_2. The Δg_1 and Δg_2 surfaces (Figure 7) are uniquely defined in terms of the mapping procedure (see eq 22) and represent *free* energies. In the range of validity of the linear response theory, where Δg_1 and Δg_2 can be approximated by harmonic functions, one can exploit the fact that $\Delta g_1 = \Delta g_2$ at the hypersurface where $\epsilon_2 = \epsilon_1$ and write (47a), where $\bar{H}_{12}$ is the

$$\Delta g^{\ddagger} \simeq (\Delta G_0 - \alpha)^2/4\alpha - \bar{H}_{12}^2(X_0)/\alpha - \bar{H}_{12}(X^{\ddagger}) \quad (47a)$$

$$|\Delta G_0| < 4\alpha$$

average of H_{12} at the indicated coordinate. The parameter α is now defined in terms of the curvature and shift of the surfaces Δg_1 and Δg_2 (see Figure 7) and is given by eq 24 when the harmonic expansion of eq 23 is valid. Outside the range of eq 47a we obtain (47b) and (47c).

$$\Delta g^{\ddagger} \simeq \Delta G_0 \qquad \Delta G_0 > 4\alpha \quad (47b)$$

$$\Delta g^{\ddagger} \simeq 0 \qquad \Delta G_0 < -4\alpha \quad (47c)$$

The correlation parameter θ is obtained from eq 47 by

$$\theta = \Delta\Delta g^{\ddagger}/\Delta\Delta G_0 \simeq (\Delta G_0 - \alpha)/2\alpha \quad (48)$$

Equation 47 without the perturbation term $\bar{H}_{12}^2/\alpha$ is identical with Marcus' equation for methyl transfer reactions (see ref 23 and 25). The problem is, however, that eq 47a is not exact, nor is it based on a fundamental microscopic principle. In fact, the Δg curves will not be harmonic for systems that do not obey the linear response approximation. Furthermore, the effective parameter α is not reproduced correctly by macroscopic estimates (see ref 16c). Even so, the solvation of ions by polar solvents can be approximated by the linear response theory, and the Δg curves can be *fitted* to a scaled quadratic relationship.[16c] Since the error range in the S_N2 simulation is larger than in our previous study[16c] of electron-transfer reactions (where $H_{12} \simeq 0$), it is hard to judge conclusively from Figure 7 how quadratic (or nonquadratic) the Δg curves are; longer simulations will be required to explore this question. Nevertheless, it appears from the present calculation that eq 47 gives a reasonable approximation provided that the key parameter α is obtained from microscopic calculations, and not from phenomenological macroscopic relationships where the cavity radius is not uniquely defined. In this respect, it is important to mention that α can be estimated quite reliably by the same approach that led to eq 43. That is, the $\Delta G(\lambda^{\ddagger})$ for our mapping potential is given by the intersection of the Δg curves. For harmonic Δg curves one obtains (49). Using this equation and

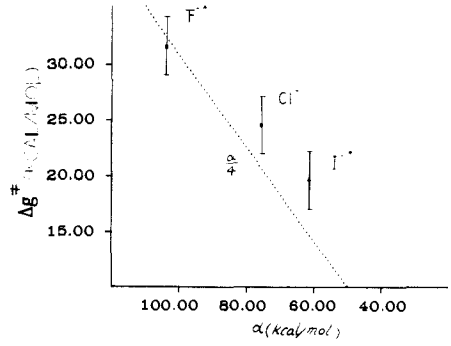

Figure 10. Dependence of the activation barrier $\Delta g^{\ddagger}$ for the symmetric exchange reaction $X^-CH_3X \rightarrow XCH_3X^-$ on the solvation energy of X^-. In order to extract the pure solvent contribution, we changed only the van der Waals solute–solvent parameters of the indicated idealized ions $(X^-)^*$ and kept the intermolecular solute potential unchanged.

eq 45 for exchange reactions ($\Delta G_0 = 0$) gives (50). This powerful relationship overcomes the need to use the ill-defined cavity radius.

$$\Delta G(\lambda^{\ddagger})_{sol} \simeq (\alpha - \Delta G_0)^2/4\alpha \quad (49)$$

$$\alpha = -2\Delta G_{sol}(X^-) - 332/R^{\ddagger} \quad (50)$$

The role of the solvent and its contribution to the overall reorganization energy can be examined by simulating several exchange reactions ($X^- + CH_3X \rightarrow XCH_3 + X^-$) where the ionic radius of the negative ion is changed in a parametric way. Such a study is described in Figure 10. The figure shows the correlation of the calculated $\Delta g^{\ddagger}$ with the calculated reorganization energy for three exchange reactions. In these three reactions the same intramolecular potential is used, while the ionic radius of X^- is modified to reproduce the observed solvation free energies of F^-, Cl^-, and I^-. Employing the same intramolecular potential in all three cases guarantees that the entire change in $\Delta g^{\ddagger}$ is due to solvation effects. A comparison of Figure 10 to direct experimental information requires one to consider the *change* in $\Delta g^{\ddagger}$ between the solution- and gas-phase reactions and to take into account the change in α due to the change in the $X^-\cdots X$ distance. This interesting taks is not, however, within the scope of the present study. Hence, we use this calculated correlation as an "experimental" microscopic check of the validity of eq 47. That is, for exchange reactions ($\Delta G_0 = 0$) one obtains (51), which gives (52). The validity of this correlation is examined in a preliminary way in Figure 10.

$$\Delta g^{\ddagger} = \alpha/4 - H_{12} - H_{12}^2/\alpha \quad (51)$$

$$\Delta\Delta g^{\ddagger}/\Delta\alpha = 1/4 + H_{12}^2/\alpha^2 \simeq 1/4 \quad (52)$$

(b) Effect of Solvent and Solute Polarizabilities. A consistent treatment of chemical reactions in solution requires one to take into account the effect of solvent polarizability. In order to examine the importance of this factor, we repeat the calculations with a model that does not include induced dipoles. Both models are parameterized to give the same solvation free energy for the Cl^- ion, by adjusting the $O\cdots Cl^-$ van der Waals radius. The results of the calculations are summarized in Figures 7 and 8. It appears that the inclusion of the solvent-induced dipoles reduces the reorganization energy by about 3 kcal/mol. This is due to the stabilization of the nonequilibrium excited diabatic states (ϵ_2 for mapping with $\Delta\epsilon > 0$ and ϵ_1 for $\Delta\epsilon < 0$) by the solvent-induced dipoles. The small induced-dipole effect might seem to justify neglecting the solvent-induced dipoles. This, however, would be permissible only for reactions that involve a charge transfer over a small distance. The same type of calculations for a hypothetical charge separation reaction ($ClCl \rightarrow Cl^-Cl^+$ with 5-Å charge separation distance) gave a reduction of $\simeq$30 kcal/mol as a result of including the solvent-induced dipoles.

Another point that requires special attention is the effect of the solvent on the solute polarization. While it is possible to use gas-phase calculations to obtain the charge distribution of the solute as a function of nuclear coordinates only, we feel that a more physically realistic picture of the reaction is obtained if the charge distribution is allowed to be changed by the (quite large) field generated by the solvent dipoles. The effect of the solvent polarization on the solute charges is the major factor in cases of charge separation reactions (e.g., Figure 1) and can be significant for S_N2 reactions. The demonstration of the importance of this effect is left to subsequent works on charge separation reactions. For the S_N2 reaction this point is demonstrated in the next section by simulating dynamical effects with and without the solute polarization.

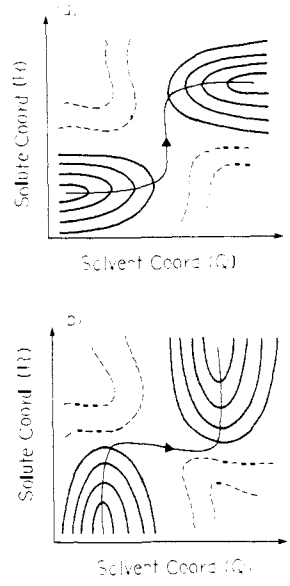

Figure 11. Hypothetical free energy surfaces for (a) the solvent-driven and (b) the solute-driven cases.

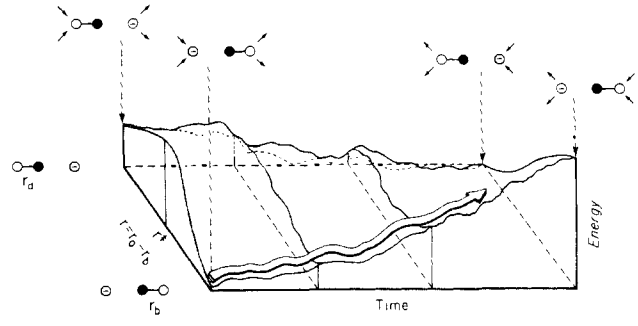

Figure 12. Schematic description of the role of the solvent fluctuations in controlling the activation barrier for the solute coordinate. The reaction occurs only when a solvent fluctuation stabilizes the reactant state and reduces the barrier along the solute coordinate.

(c) Dynamical Effects and the Key Role of Solute–Solvent Coupling. The emphasis in our study of dynamical effects is on the nature of the solute–solvent coupling. We start by considering the nature of the rare fluctuations that lead to a reactive events. In particular, it is important to determine whether the reactive fluctuations are driven by solvent fluctuations, by solute fluctuations, or by concerted solute–solvent fluctuations. This fundamental question (see related discussion in ref 26) is addressed in Figure 11. In the "solvent-driven" limit, the reaction does not occur until the solvent reaches a polarization that stabilizes either the charge distribution of the transition state or the product state and the activation barrier along the solute coordinate becomes small. In the "solute-driven" limit the solute changes its configuration (and charge distribution) to that of the transition state, while the solvent responds by moving toward its transition-state polarization. If the system follows one of these limiting cases, it is possible to consider a simplified approximation for the reaction rate. For example, in the class of solvent-driven processes, one can use the conceptual model given in Figure 12 and in our previous studies (Figure 4 of ref 18a), where the activation barrier

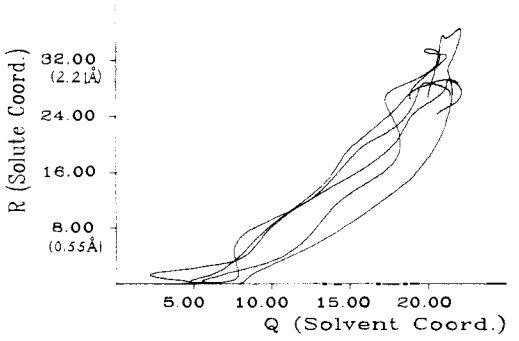

Figure 13. Nature of typical downhill trajectories for the $Cl^- + CH_3Cl \rightarrow ClCH_3 + Cl^-$ exchange reaction. The system was initialized by equilibrating the system at its transition state using $\epsilon = 0.5\epsilon_1 + 0.5\epsilon_2$. After the initial equilibration the potential was changed to the actual ground-state potential, and the system was allowed to freely evolve in time. The position of the solute coordinate is plotted as a function of the solvent coordinate, with the time entering in an implicit manner since as one moves along the curves to the right time is increasing. (This is actually a projection of a three-dimensional graph onto two dimensions with the time dimension supressed; compare to Figure 15.) The solute coordinate R is defined as $R = 0.17(\mu\nu)^{1/2}(b_2 - b_1)$, where μ is the reduced mass ($\mu = M_{Cl}M_C/(M_{Cl} + M_C)$ (amu), ν is taken as 800 cm^{-1} (which is approximately the stretching frequency of a C–Cl bond), and the meanings of b_1 and b_2 (Å) are given in Figure 5. The solvent coordinate Q is defined as $Q = (2\Delta\epsilon_{el}/h\nu)^{1/2}$, where $\nu = 100$ cm^{-1} is the effective frequency obtained from the power spectrum of $\Delta\epsilon_{el}$ and $\Delta\epsilon_{el} = (\epsilon_2 - \epsilon_1)_{el}$ is the electrostatic contribution to the energy gap between the two states used in our calculations.

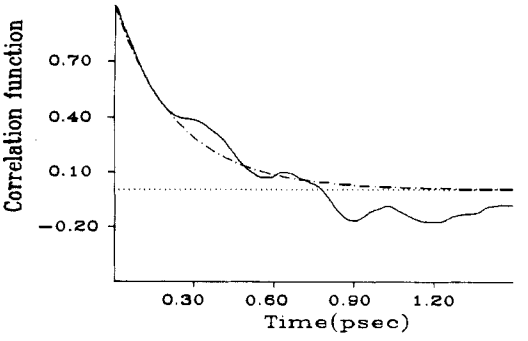

Figure 14. Autocorrelation function (solid line) of the energy gap, $\Delta\epsilon_{el}$, for the $Cl^- + CH_3Cl \rightarrow ClCH_3 + Cl^-$ reaction, which was propagated at the transition state on the mapping potential $0.5\epsilon_1 + 0.5\epsilon_2$. The simulated correlation function is compared with the function $\exp(-t/\tau_L)$ (---), where τ_L is the macroscopic dielectric relaxation time of the solvent ($\tau_L = 0.23$ ps).

along the solute coordinate fluctuates as a result of the solvent fluctuations. In this way one can obtain the activation free energy for the reaction by evaluating the probability of the solute reaching its transient transition state, $R^*(Q)$, over the solvent fluctuations.[16a] That is

$$\exp[-\Delta g^*\beta] \simeq \int \exp[-\Delta E(R_0 \rightarrow R^*, Q(t))\beta]\, dt \quad (53)$$

In fact, this approximation might be valid over a wider range (see ref 16a and 18a), since eq 53 can be thought of formally as the result of a calculation in which the solute is constrained to stay at R_0 and the probability of reaching R^* is evaluated by an umbrella sampling procedure. However, one would expect to obtain different transmission factors with eq 53 (and varying degrees of convergence) in the different limits of the solute–solvent dynamical coupling.

Regardless of the exact relationship between the nature of the reactive trajectories and the validity of eq 53, one would like to understand the dynamics of the solute–solvent coupling from a mechanistic point of view. Furthermore, different limits may show different behavior in terms of isotope effects and dependence on the dielectric relaxation of the solvent. A convenient way to explore the complicated nature of the reactive trajectories is provided by propagating trajectories downhill from the transition-state region. The time reversal of these trajectories generates the relevant set of reactive trajectories. The downhill trajectories are generated by using the mapping potential with $\lambda = \lambda^*$ to prepare the system in the transition-state region and then initiating a relaxation process by changing the potential of the system from ϵ_{m^*} to the actual ground-state potential E_g. Figure 13 describes typical downhill trajectories. As seen from the figure, the situation in our model reaction is not simple. Some trajectories seem to be solvent driven and some concerted or solute driven. In all cases, however, the solvent coordinate does play a central role. Some aspects of the solvent fluctuations will be explored below, but a more complete examination would require running many more downhill trajectories as well as an evaluation of the actual free energy along the solute and the solvent coordinates.

While the exact value of $\langle Q(t)\rangle$ requires propagating much more downhill trajectories, it is instructive to examine the dynamics of the average coordinate by the acf of $Q(t)$ and the linear response approximation of eq 37. To do this, we evaluate the acf of $Q(t)$ (Figure 14). The simulated autocorrelation time is about 0.23

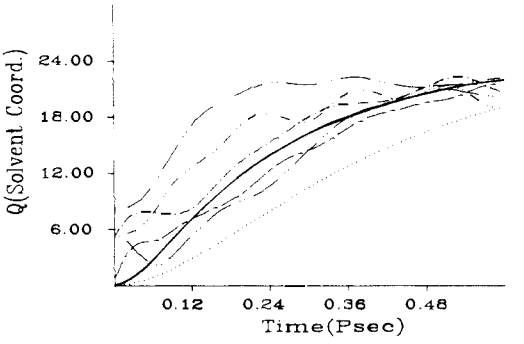

Figure 15. Time dependence of the solvent coordinate, Q, for the downhill trajectories of Figure 13. The (−··−) lines represent the actual simulation results while the (—) and (···) curves are the estimated $\langle Q\rangle$ from the model of eq 54. The (—) curve represents a model with consistent solute–solvent coupling while the (···) curve is a result of an inconsistent calculation; see text for details.

ps in good agreement with the estimate[44] of 0.23 ps for the solvent longitudinal dielectric relaxation time τ_L (a simulation of the macroscopic dielectric relaxation time of our model is required in order to examine the exact relationship between τ_L and τ_Q). With the simulated $\langle Q(0)\ Q(t)\rangle$ we evaluated $\langle Q(t)\rangle$ using a simplified version of eq 39 (eq 54), where $\langle\mu(t)\rangle_{calcd}$ is the average

$$\langle Q(t)\rangle = (Q_{max}/\mu_{max})\int_0^t \langle\dot{Q}(0)\ Q(t')\rangle\langle\mu(t - t')\rangle_{calcd}\, dt' \quad (54)$$

of the calculated solute dipole moment for the downhill trajectories. The calculated result is in good agreement with the simulated time dependence of $\langle Q(t)\rangle$ in Figure 15. More systematic studies will be required to examine the validity of our approach. It is clear however from the analysis presented in eq 39 and 40 that the time dependence of $\langle Q(t)\rangle$ is affected by the fact that the solute dipole is formed in a finite time.

Although the present study explores the nature of the reactive fluctuations only in a preliminary way, it provides a clear indication of the importance of the solute polarization effects. This point is described in Figure 16, which compares typical downhill trajectories with and without consistent solute polarization. In the first trajectory we use the correct ground-state surface (E_g), while in the second case we evaluate the solute charge by using the gas-phase EVB Hamiltonian (excluding the solute–solvent interaction term). The solute charge distribution calculated in this way (Figure 17) is determined entirely by the solute geometry and does not reflect the polarization of the solute by the surrounding solvent. Thus, the dynamics of the corresponding trajectories reflects the interaction of the solvent with the gas-phase charge distribution of the solute. As seen from Figure 16, the trajectories of the polarized solute move toward the relaxed ground state faster than those of the unpolarized solute. The reason is quite obvious: When the polarization effect is included, the magnitude of μ increases from zero to the fully polarized value

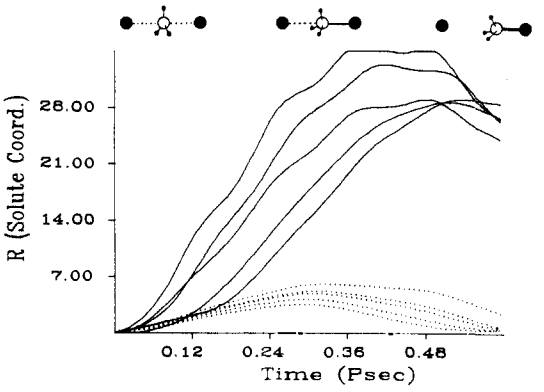

Figure 16. Time-dependent solute coordinate, R, in a typical downhill trajectory for simulations with (—) and without (···) the solute. The figure demonstrates the importance of consistent solute–solvent coupling.

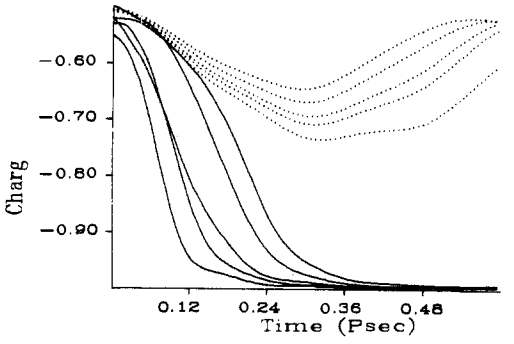

Figure 17. Charge on the attacking chlorine atom as a function of time for the trajectories given in Figure 13. (—) and (···) indicate simulations with and without including the solvent in the solute Hamiltonian.

faster than when the polarization effect is not included. The larger μ is, the stronger the relaxation force on the reaction field. The importance of this effect is also shown in an instructive way in Figure 15, which compares the results of the approach for the $\langle\mu\rangle$ calculated with and without the effect of the solute polarization. As seen from the figure, the solvent responds in a slower way in the inconsistent treatment.

IV. Concluding Remarks

Computer simulation approaches can provide detailed microscopic insight into chemical processes in the condensed phase. However, the exploitation of such approaches in a consistent and systematic way is far from being trivial. In particular, it is not clear how to incorporate both the solute and the solvent in the quantum mechanical calculations of the reacting system. Calculations that explicitly include all degrees of freedom of both solvent and solute are still well beyond the capabilities of the current generation of supercomputers. On the other hand, the use of a rigorous solute gas-phase Hamiltonian does not provide a consistent alternative to this problem (see Figure 1). Thus, it is important to develop and examine more uniform approximations that capture the main coupling between the solute and the solvent. The EVB approach described here and in our previous studies[4,16,18,19] offers a practical and consistent way of incorporating the solvent in the solute Hamiltonian. The effectiveness of this method is demonstrated here in a combined study of the energetics and dynamics of the S_N2 class of charge-transfer reactions.

A convenient combination of the EVB method and a free energy perturbation technique allows us to explore fundamental aspects of free energy relationships on a microscopic level. The method is used to examine the validity of Marcus type relationships for adiabatic charge-transfer reactions. It is found that the contribution of the solvent to the activation barrier can be estimated qualitatively with such relationships. This is due to the fact that the relevant free energy functionals can be approximated by quadratic functions, which have the same apparent dependence on the solute charges as the one obtained from macroscopic dielectric theories (provided that the reorganization energy is not evaluated using an arbitrary cavity radius, but either by microscopic calculations or by empirical scaling using eq 50 and observed solvation energies). This does not imply, however, that the macroscopic theory is rigorously valid. The previously used macroscopic models of Marcus[23] and Hush[24] evaluated free energies by using macroscopic models that constrain the electrostatic free energy to change along the reaction coordinate. Here, on the other hand, we use the *potential* energy of the constraint Hamiltonian to drive the system and *calculate* the relevant free energy from the corresponding potential energies. The two approaches are clearly not indentical; the present one is more rigorous since it actually evaluates the relevant free energies from first principles. Using the microscopic approach should give one (when the convergence error is reduced) the ability to explore the basic derivation of the macroscopic approaches and attack outstanding problems, such as the nature of the difference between the Marcus[23] and Hush[24] points of view.

The simple incorporation of the solvent field in the solute Hamiltonian is one of the key advantages of the present treatment. Inclusion of the solute–solvent coupling, which is missing in most other approaches, is more than a pedagogical exercise. While in the S_N2 class of reactions the effect of the solvent on the energetics and dynamics is rather small, it becomes a huge effect in charge separation reactions (e.g., proton-transfer processes).

The present work explores some dynamical aspects of an S_N2 reaction, emphasizing the solute–solvent coupling. An examination of the adiabatic limit reveals a nonlinear coupling, a consistent treatment of which might be essential for reliable simulation of charge transfer dynamics. It appears that the solvent response function is determined by both the solvent dielectric relaxation time and the solute polarization time. Examining this point with the linear response approximation provides some interesting insight into the dynamics of the solvent. However, several major issues are left open. In particular, it would be interesting to find out (by running many more downhill trajectories) whether or not the solvent reactive fluctuations, which are determined by the actual many-dimensional potential surfaces, can be reliably approximated by one-dimensional dynamics on the corresponding free energy functionals. Such an assumption, which is implicit in most of the current formal studies, has not been derived rigorously from first principles.

In concluding this paper we point out that despite the significant progress being made in computer simulation approaches, one can still benefit greatly from the insight provided by phenomenological models. The results of the simulation studies can be used (in conjunction with the available experimental information) to examine and to "scale" these phenomenological models. In this respect, we find the EVB method particularly useful in providing a convenient connection between the simulation studies and the relevant free energy functionals. More studies in this area will be reported in subsequent works.

Acknowledgment. This work was supported in part by Grant GM24498 from the National Institutes of Health, by the Office of Naval Research, Contract N00014-87-K-0507, and by the NSF San Diego Supercomputer Center.

Appendix A

The coupled equation of motion for the effective solute–solvent coordinate depends of course on the definition of these coordinates. A convenient definition is provided by the Q and R of section III. With this definition and the potential for Q in eq 30 we can write (A1), where $A'(t)$ is a random force and $Q = (m_Q\omega_Q/\hbar)^{1/2}Q'$. Approximating γ_Q by a δ function ($\gamma = \gamma_Q\,\delta(t)$) gives (A2), where $A = (\omega_Q/\hbar m_Q)^{1/2}A'$ and the mass m_Q can be found by the equipartion relationship (A3).

$$m_Q\ddot{Q}' = -\int_0^t m_Q\gamma_Q(t-\tau)\,\dot{Q}'(\tau)\,d\tau - \partial V/\partial Q' + A'(t) \quad \text{(A1)}$$

$$\ddot{Q} = -\gamma_Q\dot{Q} - (\omega_Q/\hbar)\,\partial V/\partial Q + A(t) \quad \text{(A2)}$$

$$m_Q = k_BT/\langle\dot{Q}^2\rangle \quad \text{(A3)}$$

The friction term can be obtained from the acf of $\dot{Q}$ by[41] (A4), and $A(t)$ is related to γ_Q by the fluctuation dissipation theorem.[41]

$$\gamma_Q = (k_B T/m_Q)\left(\int_0^\infty \langle \dot{Q}'(0)\ \dot{Q}'(t)\rangle\ dt\right)^{-1} = (k_B T\omega_Q/\hbar)\left[\int_0^\infty \langle \dot{Q}(0)\ \dot{Q}(t)\rangle\ dt\right]^{-1} \quad (A4)$$

We can also use the properties of Brownian harmonic oscillator[45] to relate γ_Q to the dielectric relaxation time of the solvent. That is, the autocorrelation time of the reaction field, ξ_R, and therefore Q (see eq 26) is given (within the model of Nee and Zwanzig[42]) by the longitudinal relaxation time, τ_L, of the solvent. Although the microscopic nature of the first few solvation shells is likely to give somewhat different relaxation time, we can still use the approximation (A5), where $\omega_1^2 = \omega_Q^2 - (\gamma_Q^2/4)$.

$$\tau_L \simeq \tau_Q = \int_0^\infty \langle Q(0)\ Q(t)\rangle\ dt/\langle Q(0)\ Q(0)\rangle = \int_0^\infty e^{-\gamma_Q t/2}\left(\cos(\omega_1 t) + \frac{\gamma_Q}{2\omega_1}\sin(\omega_1 t)\right) = \gamma_Q/\omega_Q^2 \quad (A5)$$

The friction term can now be expressed as

$$\gamma_Q = \omega_Q^2 \tau_Q$$

Thus we have (A6). Similarly, we can write the approximated equation of motion of R as (A7), where we assume that the main friction and random force contribution to R comes through the dependence of E_g on Q.

$$\ddot{Q} = -\omega_Q^2\tau_Q\dot{Q} - \omega_Q^2 Q - 2(\omega_Q/\hbar)(\mu\alpha_Q/\mu_{max}\Delta_Q)[(\partial\mu/\partial Q)Q + \mu] + A(t) \quad (A6)$$

$$\ddot{R} = -\gamma_R\dot{R} - (\omega_R/\hbar)\partial E_g/\partial R + A_R(t) \quad (A7)$$

It should be instructive to compare the numerical results of eq A6 and A7 to those of the actual many-dimensional simulations. It is also interesting to find approximated analytical solutions for these equations. For example, one can consider the Smoluchowski equivalent of eq A6 (with the diffusion constant $D_Q = k_B T/(m_Q\omega_Q^2\tau_Q)$) (eq A8), where $P(Q, t)$ is the probability of finding

$$\frac{\partial}{\partial t}P(Q, t) = (m_Q\omega_Q/\hbar)\frac{\partial}{\partial Q}\left(D(Q)\left(\frac{\partial}{\partial Q} + \gamma\frac{\partial V}{\partial Q}\right)\right)P(Q, t) \quad (A8)$$

the system using the corresponding first passage approximation,[43] which reduces to Kramer's derivation.[46] In the high barrier case one obtains (A9) (see related derivations of Zusman,[48] Calef and Wolynes,[15] and Ovchinnikova[47]), where $\omega_Q^\ddagger$ is the curvature of Δg at the transition state and $\bar{D}_Q$ is the average diffusion constant.

$$k_Q(R) \simeq (\hbar/m_Q\omega_Q)^{1/2}\bar{D}_Q\left[\int_\infty^0 dQ[\exp(-\Delta g(Q, R)\beta)/Z]^{-1}\right]^{-1} \simeq (\omega_Q^\ddagger/\omega_Q)(2\pi\tau_Q)^{-1}\exp(-\Delta g^\ddagger(R)\beta) \quad (A9)$$

The problem is, however, that in contrast to the simple case of diabatic electron transfer we deal here with a strong coupling of Q and R as well as with the complicated form of μ. A rather rough approximation can be obtained for the solvent-driven case by taking k as the value $k_Q(R)$ at the ground-state value of R. More sophisticated approximation may be obtained by introducing the time-dependent effect of R in eq A7 as a memory kernel (see related treatments in ref 13a and b). Possible manipulations of eq A9 will be examined in subsequent work. In the present study (section IIIC) we explore the solute–solvent coupling by using the linear response theory.

Appendix B

The relation between the rate constant and the fluctuations of the time-dependent energy gap can be explored by exploiting some of the formalism used in the diabatic limit.[16b] The idea is to find the number of times, $n(X^\ddagger, \tau)$, the system reaches the transition state during a given time τ by finding functionals whose stationary points occurs at the transition state. To do this we start by expressing the forward rate constant as (B1). To find $n(X^\ddagger)$ we use the function (B2), where $\Delta\epsilon = \epsilon_2 - \epsilon_1$ and $\langle\ \rangle_{g'}$ designates an average over a potential given by (B3). The reflecting boundary

$$k = (n(X^\ddagger, \tau)/\tau)F \quad (B1)$$

$$W(\tau) = \left\langle\left|\int_0^\tau \exp\left[\left(-i/\hbar\int_0^t \Delta\epsilon(t')\ dt'\right)\right]\right|^2\right\rangle_{g'} \quad (B2)$$

$$E_{g'} = E_g \qquad X \le X^\ddagger \quad (B3)$$

$$E_{g'} = E_g(X^\ddagger)[1 + \exp[(X - X^\ddagger)]] \qquad X > X^\ddagger$$

of this potential guarantees that the trajectories of the system will spend almost all of the time at the reactant state. The same type of functional was in fact used in the diabatic limit[16b] using an average over ϵ_1. However, the actual relation of $W(\tau)$ to the rate constant is much less obvious in the adiabatic case. Here we cannot follow the diabatic derivation[16b] and assume that the system stays in the state ψ_1 throughout the investigation time. However, we can exploit the fact that the functional $W(\tau)$ still provides an estimate of $n(X^\ddagger, \tau)$, since the rapidly oscillating integral in eq B2 contributes to $W(\tau)$ only when $\Delta\epsilon = 0$. Thus, we can write (B4), where the factor $\Gamma(\dot{X}^\ddagger) = |2\pi\hbar/\Delta\dot{\epsilon}|$ (which is related to the Landau–Zener factor in the diabatic derivation) is obtained as in ref 16b by the stationary-phase approximation, while the phase ϕ_j is given by the integral of the energy gap between t_j to t_{j+1} (see ref 16b). Following the argument of ref 16b and the related argument of Feynman[49] about phase cancellation between different trajectories, one can write[16b] (B5). Using eq B1 and B5 we obtain (B6). The factor F still appears in our expression since the stationary-phase approximation of eq B4 does not allow trajectories to bounce back after crossing the transition state. This treatment does not change the results of the diabatic treatment[16b] where the surface crossing probability is very small so that most trajectories that cross never come back (as argued in ref 57 the fraction of trajectories that return is $\theta/(2-\theta)$, where θ is the surface crossing probability).

$$W(\tau) = \left\langle\left|\sum_{j=1}^{n(X^\ddagger,\tau)}\int_{t_j}^{t_{j+1}}\exp\left[-i/\hbar\int_0^t\Delta\epsilon(t')\ dt'\right]dt\right|^2\right\rangle_{g'} = \left\langle\left|\sum_{j=1}^{n(X^\ddagger,\tau)}\Gamma(\dot{X}^\ddagger)^{1/2}e^{i\phi_j}\right|^2\right\rangle_{g'} \quad (B4)$$

$$W(\tau) \simeq \left\langle\sum_{j=1}^{n(X^\ddagger,\tau)}\Gamma(\dot{X}^\ddagger)\right\rangle_{g'} \simeq n(X^\ddagger, \tau)\langle\Gamma(\dot{X}^\ddagger)\rangle_g \quad (B5)$$

$$k = (W(\tau)/\tau)F/\langle\Gamma\rangle \quad (B6)$$

Equation B6 allows one to exploit the formal properties of $W(\tau)$ using its second-order cumulant expansion (see ref 16b) that gives (B7), where $k^{(2)}$ designates the second-order approximation for k and $\Delta\epsilon = u + \langle\Delta\epsilon\rangle$. (Note that, in contrast to the diabatic case of ref 16b, we do not perform the average over the distribution function of ϵ_1 or ϵ_2.)

$$k^{(2)} \simeq \left(\int_{-\infty}^{\infty} dt\ \exp[(i/\hbar)\langle\Delta\epsilon\rangle t + \gamma(t)]\right)F/\langle\Gamma\rangle \quad (B7)$$

$$\gamma(t) = (-1/\hbar)^2\int_0^t dt'\,(t - t')\langle u(0)\ u(t')\rangle_g$$

Equation B7 provides a direct way for exploring the relationship between the rate constant and the solvent dielectric relaxation time, which determines the acf of $\Delta\epsilon$. In fact, if we write the acf of $u(t)$ as (B8), then an analogous derivation to that of ref 16b gives, for cases with *low* $\Delta g^\ddagger$ where $\langle\Delta\epsilon\rangle \simeq 0$ and $\tau_u \ll \hbar/(2Ak_BT)^{1/2}$, the relationship (B9). The difference, however, from the diabatic

$$\langle u(0)\ u(t)\rangle_g = 2Ak_bTe^{-t/\tau_u} \quad (B8)$$

$$k^{(2)} \simeq (\hbar^2/Ak_BT\tau_u)F/\langle\Gamma\rangle \quad (B9)$$

case of ref 16b is the range of validity of eq B9. In the adiabatic case the amplitude A is much smaller than in the diabatic case (where A is given by the reorganization energy α). Thus, eq B9 is expected to be valid in the adiabatic cases on a wider range of τ_u than in the diabatic cases.

The acf $\langle u(0)\, u(t)\rangle_g$ can be obtained directly by simulations. However, significant formal insight can be gained by examining analytical autocorrelation functions for a given effective equation of motion for $u(t)$. This point will be explored in subsequent publications.

How Does a Dication Lose a Proton?

Peter M. W. Gill and Leo Radom*

Contribution from the Research School of Chemistry, Australian National University, Canberra, A.C.T. 2601, Australia. *Received October 29, 1987*

Abstract: A detailed study of the mechanism by which a proton is lost from a dication reveals that such processes are more complicated than is often assumed. In many cases, a deprotonation reaction is best viewed as a two-stage process: Initially, the departing unit is better described as a hydrogen atom than as a proton and only later, at some point further along the decomposition pathway, does a spontaneous electron transfer take place to form the eventual products. Consequently, it is found that, contrary to conventional wisdom, *restricted* Hartree–Fock (RHF) theory does not necessarily offer a satisfactory theoretical treatment of such fragmentations. The circumstances under which it is appropriate to use RHF or UHF procedures (and the Møller–Plesset perturbation theories based on these) are examined in light of a recent model for dication dissociation, and it is found that the Δ parameter of that model is a useful aid in choosing the theoretical formalism appropriate to a given dication.

The chemistry of gas-phase dications has received considerable attention in recent years, from both theoreticians and experimentalists.[1] Such species are usually thermodynamically unstable with respect to dissociation into two monocations, but significant kinetic stability may result if sufficiently high barriers impede fragmentation. For this reason, the accurate assessment of such barriers is of paramount importance in the theoretical investigations of dications.

One ubiquitous fragmentation route for dications is proton loss (eq 1). The observation that the transition structure for such

$$AH^{2+} \rightarrow A^{+} + H^{+} \qquad (1)$$

reactions often occurs very late along the reaction path has recently been rationalized[3] in terms of a model[2-4] in which the potential curve for the fragmentation is viewed as arising from an avoided crossing between an ion–ion repulsive state, which correlates with $A^+ + H^+$, and an ion–induced-dipole attractive state, which correlates with $A^{2+} + H$. This model may be used, for example, to show that if the second ionization energy of A is a little larger than 13.6 eV (the ionization energy of H), a late-transition structure for proton loss may be anticipated.

Further inspection of this model can give considerable insight into the dissociation process and reveals certain features that have previously been overlooked. In particular, if AH^{2+} is a closed-shell singlet species, it is conventionally assumed[5] that the proton loss may be treated within the framework of restricted (RHF), as opposed to unrestricted (UHF), Hartree–Fock theory. However, as we show in this paper, the choice between these alternatives is less straightforward than is normally realized, and indeed, for late-transition structures, RHF ought not be used.

Table I. Calculated Bond Lengths (Å) and Total Energies (Hartrees) of the Equilibrium and Transition Structures of AlH^{2+} and Corresponding Barriers for Deprotonation (kJ mol^{-1})[a]

	r_{eq}	E_{eq}	r_{TS}	E_{TS}	barrier[b]
RHF	1.614	−241.562 64	3.009	−241.511 15	135
RMP2	1.641	−241.595 18	3.118	−241.549 00	121
RMP3[c]	1.653	−241.594 39	3.169	−241.545 43	129
RMP4[c]	1.660	−241.597 29	3.142	−241.549 39	126
RCISD[c,d]	1.669	−241.599 80	3.206	−241.550 29	130
TCSCF[e]	1.671	−241.589 99	3.415	−241.530 45	156
UHF	1.645	−241.562 84	3.589	−241.520 68	111
UMP2	1.641	−241.595 18	3.309	−241.539 53	146
UMP3[c]	1.653	−241.594 39	3.276	−241.533 97	159
UMP4[c]	1.660	−241.597 29	3.250	−241.535 72	162
UCISD[c,d]	1.669	−241.599 80	3.206	−241.550 23	130

[a] 6-31G* basis set used throughout. [b] $E_{TS} - E_{eq}$. [c] Frozen-core approximation used. [d] Corresponds to full CI for the valence electrons. [e] 4σ and 5σ molecular orbitals were active.

Method and Results

A modified version[6] of the GAUSSIAN 82 system of programs[7] was used to carry out standard ab initio calculations[8] on AlH^{2+} and $N_2H_6^{2+}$ with the 6-31G* basis set, both for the equilibrium structures and for the transition structures for deprotonation. The equilibrium and transition structure bond lengths in AlH^{2+} were optimized at the Hartree–Fock (HF), second-, third-, and fourth-order Møller–Plesset perturbation theory (MP2, MP3, and MP4, respectively), and singles-and-doubles configuration interaction (CISD) levels, within both the spin-restricted (leading to RHF, RMP, and RCISD) and spin-unrestricted (leading to UHF, UMP, and UCISD) frameworks. The bond lengths were also optimized at the two-configuration SCF (TCSCF) level with the 4σ and 5σ molecular orbitals as the active space. The results, including corresponding barrier heights, are summarized in Table I. Because AlH^{2+}

(1) For recent reviews, see: (a) Koch, W.; Maquin, F.; Stahl, D.; Schwarz, H. *Chimia* **1985**, *39*, 376. (b) Koch, W.; Schwarz, H. In *Structure/Reactivity and Thermochemistry of Ions*; Ausloos, P., Lias, S. G., Eds.; NATO ASI Series; Reidel: Dordrecht, The Netherlands, 1987.
(2) Dorman, F. H.; Morrison, J. D. *J. Chem. Phys.* **1961**, *35*, 575.
(3) Gill, P. M. W.; Radom, L. *Chem. Phys. Lett.* **1987**, *136*, 294.
(4) Gill, P. M. W.; Radom, L. *Chem. Phys. Lett.*, in press.
(5) For example: Schleyer, P. v. R. *Adv. Mass Spectrom.* **1985**, 287.
(6) (a) Baker, J.; Nobes, R. H.; Poppinger, D.; Wong, M. W., unpublished results. (b) Baker, J. *J. Comput. Chem.* **1986**, *7*, 385.
(7) Binkley, J. S.; Frisch, M. J.; DeFrees, D. J.; Raghavachari, K.; Whiteside, R. A.; Schlegel, H. B.; Fluder, E. M.; Pople, J. A. GAUSSIAN 82; Carnegie-Mellon University: Pittsburgh, PA, 1982.
(8) Hehre, W. J.; Radom, L.; Schleyer, P. v. R.; Pople, J. A. *Ab Initio Molecular Orbital Theory*; Wiley: New York, 1986.

0002-7863/88/1510-5311$01.50/0